The Thesis Committee for Son Dang Thai Phan

Certifies that this is the approved version of the following thesis:

Pre-injection reservoir evaluation at Dickman Field, Kansas

APPROVED BY

SUPERVISING COMMITTEE:

Supervisor: _____

Mrinal K. Sen

_____

Sanjay Srinivasan

_____

Stephen Grand

Pre-injection reservoir evaluation at Dickman Field, Kansas

By

Son Dang Thai Phan, B.S.

Thesis

Presented to the Faculty of the Graduate School of

The University of Texas at Austin

In Partial Fulfillment

Of the requirements

For the Degree of

Master of Science in Geological Sciences

The University of Texas at Austin

August 2011

Dedication

To my parents,

Liem Thanh Phan and Hanh Dang Thi Ngoc

Acknowledgements

I would like to thank my supervisor, Professor Mrinal K. Sen for his inspiration, encouragement and discussion throughout my graduate studies. I would also like to thank Dr Sanjay Srinivasan and Dr Stephen Grand for serving on my committee and for suggestions to improve the thesis.

I would like to express my sincere thank to Professor Christopher Liner from The University of Houston for providing me with the essential data to fulfill my research. I also thank other research scientists at the Institute for Geophysics and at Department of Geological Sciences for their help with my work.

I would like thank my friends and colleagues at The University of Texas at Austin for their great support: Sayantan Bhowmik, Ankesh Anupam, Nhat Minh Nguyen, Mohammed Al Hussain, Corey Joy, Yi Tao, Yang Xue, Ranjana Ghosh. My special thanks go to Samik Sil for helpful discussions on the objects, Thanh Nguyen from CMG for helping me with simulation software.

Many thanks to Mark Wiederspahn and Steffen Saustrup for their technical support, and Phillip Guerrero from the Department of Geological Sciences for useful advice.

I would also like to acknowledge various sources of financial support during my graduate studies: the Center for Frontiers of Subsurface Energy Security, an Energy Frontier Research Center funded by the US Department of Energy, Office of Science, Office of Basic Energy Sciences under Award Number DE-SC0001114; the Chevron-Texaco Fellowship and the support from The Department of Geological Sciences, The University of Texas at Austin.

Finally, I would like to thank my parents and family for their endless love and warm support.

August 2011

Abstract

Pre-injection Reservoir Evaluation at Dickman Field, Kansas

By

Son Dang Thai Phan, M.S.Geo.Sci.

The University of Texas at Austin, 2011

SUPERVISOR: Mrinal K. Sen

I present results from quantitative evaluation of the capability of hosting and trapping CO_2 of a carbonate brine reservoir from Dickman Field, Kansas. The analysis includes estimation of some reservoir parameters such as porosity and permeability of this formation using pre-stack seismic inversion followed by simulating flow of injected CO_2 using a simple injection technique.

Liner et at (2009) carried out a feasibility study to seismically monitor CO_2 sequestration at Dickman Field. Their approach is based on examining changes of seismic amplitudes at different production time intervals to show the effects of injected gas within the host formation. They employ Gassmann's fluid substitution model to calculate the required parameters for the seismic amplitude estimation. In contrast, I employ pre-stack seismic inversion to successfully estimate some important reservoir parameters (P- impedance, S- impedance and density), which can be related to the changes in subsurface rocks due to injected gas. These are then used to estimate reservoir porosity using multi-attribute analysis. The estimated porosity falls within a reported range of 8-25%, with an average of 19%. The permeability is obtained from porosity assuming a simple mathematical relationship between porosity and permeability and classifying the rocks into different classes by using Winland R35 rock classification method. I finally perform flow simulation for a simple injection technique that involves direct injection of CO_2 gas into the target formation within a small region of Dickman Field. The simulator takes into account three trapping mechanisms: residual trapping, solubility trapping and mineral trapping. The flow simulation predicts unnoticeable

changes in porosity and permeability values of the target formation. The injected gas is predicted to migrate upward quickly, while it migrates slowly in lateral directions. A large amount of gas is concentrated around the injection well bore. Thus my flow simulation results suggest low trapping capability of the original target formation unless a more advanced injection technique is employed. My results suggest further that a formation below our original target reservoir, with high and continuously distributed porosity, is perhaps a better candidate for CO_2 storage.

Table of content

List of Tables

List of Figures

Chapter 1: Introduction

1.1 Carbon Sequestration

Carbon Sequestration aims at reducing green-house gas emission by injecting carbon dioxide (CO_2) into an underground formation with good trapping and storage capability. Storage is defined as permanent only if 99% of the injected CO_2 remains securely confined after 100 years (NETL 2007). The storage efficiency cannot be assured without the development of reliable and highly accurate leakage monitoring, plume detection and monitoring, and volume accounting technologies (Sayers et al 2010). Well logs are high-resolution records of subsurface rock properties but are limited to a few spatial locations only. On the other hand, seismic data though of poor vertical resolution, have wide spatial coverage. In addition characteristic changes in seismic wave patterns can be identified that can be attributed to changes in fluid content of a rock. Thus seismic data has tremendous potential of imaging subsurface fluid flow through time-lapse seismic monitoring. In essence, Seismic monitoring of CO_2 storage and movement underground relies on our understanding of the systematic changes, if any, of elastic properties of subsurface rock layers.

One way of examining the effect of CO_2 in subsurface rocks is to measure elastic properties of rocks in the laboratory. For example, Vanorio et al (2009) examined a rock physic model to predict the acoustic properties of a CO_2 rich solution under subcritical condition, and to simulate the changes in velocities (P- wave velocity and S- wave velocity) when this solution is injected into a reservoir. The results show that Vp and Vs both decrease with increased injected volume of CO_2 due to changes in porosity and chemical precipitation. Most recently, Ghosh and Sen (2011) developed a new frequency-

dependent effective medium model to predict elastic properties that include the effects of dispersion and chemical precipitation.

There exist a few field studies of seismic monitoring of CO_2. For example, Chadwick and his team applied many quantitative methods to the Sleipner Seismic data set to monitor the CO_2 plume movement. The flow simulation during early states of gas injection (Chadwick et al 2005) suggested 10% of the free gas to be dissolved into the aqueous phase. The uncertainty in seismic interpretation of the dataset states the difficulty in characterizing the deeper plume as its amplitude is diminished and a pushdown of velocity is caused by the distribution of injected CO_2. The post-stack seismic inversion (Delepine et al 2009) predicts a strong reduction in P-wave impedance. Meanwhile, the spectral decomposition and extrema analysis successfully classified the thickness of the CO_2 layer. Further study at Sleipner Field involves more advanced quantitative analysis of time-lapse seismic and full waveform inversion in frequency domain to improve the estimation of CO_2 layer thickness.

Urosevic et al (2009) employed time lapse seismic to monitor CO_2 injection into a depleted CH_4 gas reservoir at Naylor Field, Australia. The challenging conditions of the site require the engagement of nonconventional source and recording geometries. Also the residual gas saturation near injection zone does not present a favorable condition for seismic monitoring. Despite those difficulties, the time-lapse seismic analysis produced promising results with high repeatability by using two different and low- energy output sources. The amplitude contrast caused by the introduction of CO_2 into the formation is detectable.

Ma et al (2009) monitored the movement of injected CO_2 in a carbonate reservoir at Wayburn Field, Canada by applying the fluid substitution model based on Gassmann's equation. They combine the effective porosity with the shale content correction to correct for changes in real well logs after gas is injected into the formation. The synthetic seismograms calculated by using the exact Zeoppritz equation correctly reflects the changes in seismic amplitudes with offset under the influence of injected gas. However, the robustness and stability of the modeled reservoir are low due to the nonlinearity and acute sensitivity of the AVO response to CO_2 saturation.

Zarantonello et al (2009) presented their result on the effectiveness of seismic imaging for monitoring CO_2 sequestration within a coal formation. The study considered two scenarios: (1) injected gas remaining confined within the coal formation, (2) the gas leaked through semi-permeable shale layer above the sealed sand unit. The synthetic seismograms are generated by simulating wave propagation through a media assuming some rock physics and geo-statistical dual-porosity model of the coal, sand and shale units, and Reverse Time Migration (RTM) to reconstruct 3D images of the reservoir at the beginning and the end of the injection process. The resulting images show significant contrast in seismic amplitude of the CO_2 gas saturated zone. However, their approach does not address the differentiation in seismic signatures of CO_2 and CH_4 gas.

Although there exists some successful case studies of CO_2 monitoring, the quest for an effective, robust and repeatable technique to monitor CO_2 injection is still on going.

1.2 Problem Statement

As stated earlier, CO_2 sequestration has been applied successfully in several places around the world. It requires injecting CO_2 into geologic formations, which are capable of trapping and containing CO_2 with the lowest risk of leakage. After injection, it requires seismic imaging and interpretation to monitor the behavior of injected CO_2 within the target horizons. However, due to the differences in geological settings of different areas, the details of seismic investigations required at those areas are different. My research focuses on a carbonate reservoir at Dickman Field, Kansas (Figure 1.1). The target layer for CO_2 injection in this area is a Mississippian carbonate brine reservoir (Figure 1.2).

The dataset used in this study was collected with funding from the Department of Energy (DOE). Liner et al (2009), in their preliminary analysis, employed Gassmann fluid substitution equation, which requires knowledge of the porosity distribution within the target reservoir along with some other petro-physical properties (rock type, fluid content etc.), to study the sensitivity of seismic monitoring for CO_2 sequestration at Dickman Field by looking at the changes of synthetic seismic amplitudes at different production time intervals. They converted seismic volumes from time to depth for well calibration and reflectivity estimation. Reservoir parameters such as pressure, temperature, velocity, and water saturation were estimated from the depth section of well logs, and used as input to Gassmann's equation to estimate bulk modulus. These were then used for impedance calculation followed by reflectivity calculation. The result is a volume of synthetic traces whose amplitudes are controlled by CO_2 saturation.

Unlike the approach taken by Liner et al (2009), I use the same seismic data to quantitatively estimate some important reservoir parameters such as porosity and

permeability of this formation. My analyses include pre-stack velocity analysis, pre-stack inversion and mapping of inversion results to porosity by a multi-attribute linear regression algorithm. Note that porosity is one of the most crucial parameters in assessing different scenarios when injecting CO_2 within this reservoir. I then calculate permeability using calculated porosity assuming a mathematical relationship between those two parameters. Next I incorporate my petro-physical results in a reservoir simulator to investigate different time- lapse scenarios. The overall result from this study is useful in determining the capability of the host rock to host the injected CO_2. The method used in this study can also be applied for seismic monitoring of CO_2 injection used for Enhanced Oil Recovery.

1.3 Study Area

1.3.1 Location and Geological Setting

My study focuses on a carbonate reservoir at Dickman Field, which is located at Ness County, Kansas (Figure 1.1). Three major geological events can be identified at Dickman Field, namely, the Mississippian-Pennsylvanian deposition (Liner 2009): the deposition of Middle-Upper Mississippian shelf carbonates, the exposure of Middle-Upper Mississippian Strata associated by karst-development and the deposition of Pennsylvanian Coal-bearing formations over the Mississippian Unconformity. They are affected by the continental collision at the South of the area, from 335 to 310 million years (Ma).

Figure 1.3 shows a lithological cross section of the Dickman Field, where the section is hung on Fort Scott Limestone top. The horizons are named after smaller time scale geological events. From oldest to youngest, they are:

- Post-Gilmore City exposure along with early stage of karst development; the deposition of Osage Strata on Gilmore City and its exposure (short term) resulting in fractures parallel or vertical to bedding, and pressure solution zones in deep saline aquifer
- The deposition of Warsaw-Salem carbonate strata on shelf and its Post Mississippian exposure associated with mature karst development, erosion and tunnels collapsed
- The deposition of Lower Cherokee Cherty Conglomerate and Sandstone within relic channels on Mississippian Unconformity, resulting in a sandstone reservoir
- The formation of Fort Scott Limestone as sealing layers from the interwoven cyclic of carbonate shelf and coastal swamp facies
- Series of Post-Pennsylvanian folding, fracturing and faulting resulting in the lifting and tilting of Mississippian and Pennsylvanian Fort Scott strata

1.3.2 Data

The University of Houston collected a 3D seismic data set, which includes pre- and post-stack volumes, at the Dickman Field. The coverage of seismic data on the surface is in an irregular shape that contains 158 in-lines spaced at 82.5 ft running North South, and 127 cross-lines spaced at 110 ft running East West (Figure 1.2). The maximum fold of a CMP is 60. Although many wells are available in the area, only four of them contain sonic and/or density data, and neutron porosity log. Those are essential well logs that control the quality of results needed for my study, and they will be discussed further in the next section. The four wells are Humphrey 4-18, Dickman 1, Dickman 6, Elmore 3. Their locations and types of logs are listed in Table 1. There are

several geological horizons that have been picked in SMT Kingdom from The University of Houston, and I am using four of them. The horizons are FortScott Limestones, Mississippian Carbonate, Viola and Gilmore City formation.

1.3.3 *A Priori* Information

Dickman Field used to be an oil-producing field. The majority oil reserve is from the Mississippian Carbonate zone. The production has stopped and the field has become an oil-depleted field. The saline aquifer under Dickman Field is part of the Western Interior Plains Aquifer and Ozark Plateaus Aquifer (Liner 2009). The salinity at Ness County is about 45,000 ppm.

The target formation is a Mississippian Carbonate formation. In time domain, it is 800ms-900ms below the surface. Primary study from Liner (2009) reveals that the Mississippian reservoir porosity ranges from 8% to 25%, with an average of 21%. The reservoir core has a high water saturation ranging from 35% to 70%. Dickman Field data set contains no further a priori information regarding.

1.4 Thesis Organization

In Chapter 2, I describe the method and results from fractal based Pre-stack seismic inversion using a simulated annealing approach called Very Fast Simulated Annealing (VFSA) algorithm, which was introduced by Srivastara and Sen (2010). Detail processing steps are listed in the order that I approach the study. Sequentially, in Chapter 3, I describe estimation of the porosity and permeability of the target formation using some statistical and mathematical algorithms that combine the results from the inversion described in Chapter 2. The subsequent chapter progresses with the simplest flow simulation algorithm called CMG simulator from Computer Modeling Group (CMG) to

try to predict the behavior of CO_2 when it is injected into the reservoir. The last chapter includes general conclusions of this study and suggests some future works that can be done after this study. Each chapter begins with a brief introduction of the process in terms of model parameters, available data and preparation and some a priori information. Appendix A provides a summary of the technical aspects of the seismic inversion approach (VFSA- Srivastava and Sen (2010)) used in my thesis.

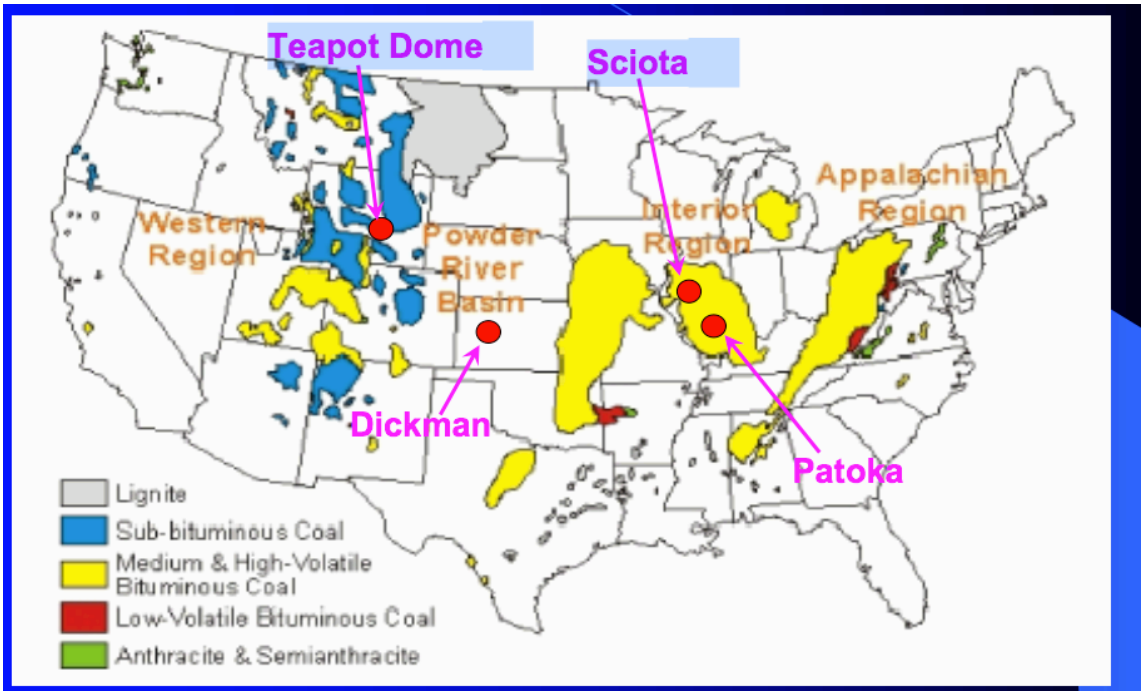

Figure 1.1: Location of Dickman field in Central America

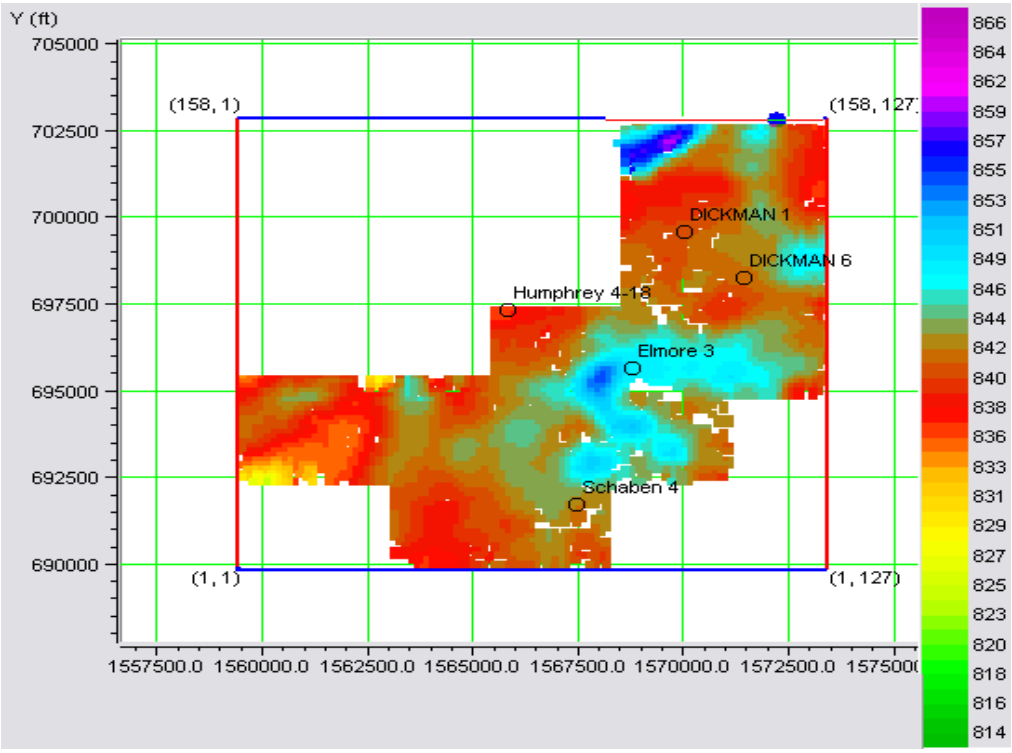

Figure 1.2: Time slice of the Mississippian carbonate displays a contour plot of seismic amplitude at the horizon, irregular survey boundary is apparent in the figure.

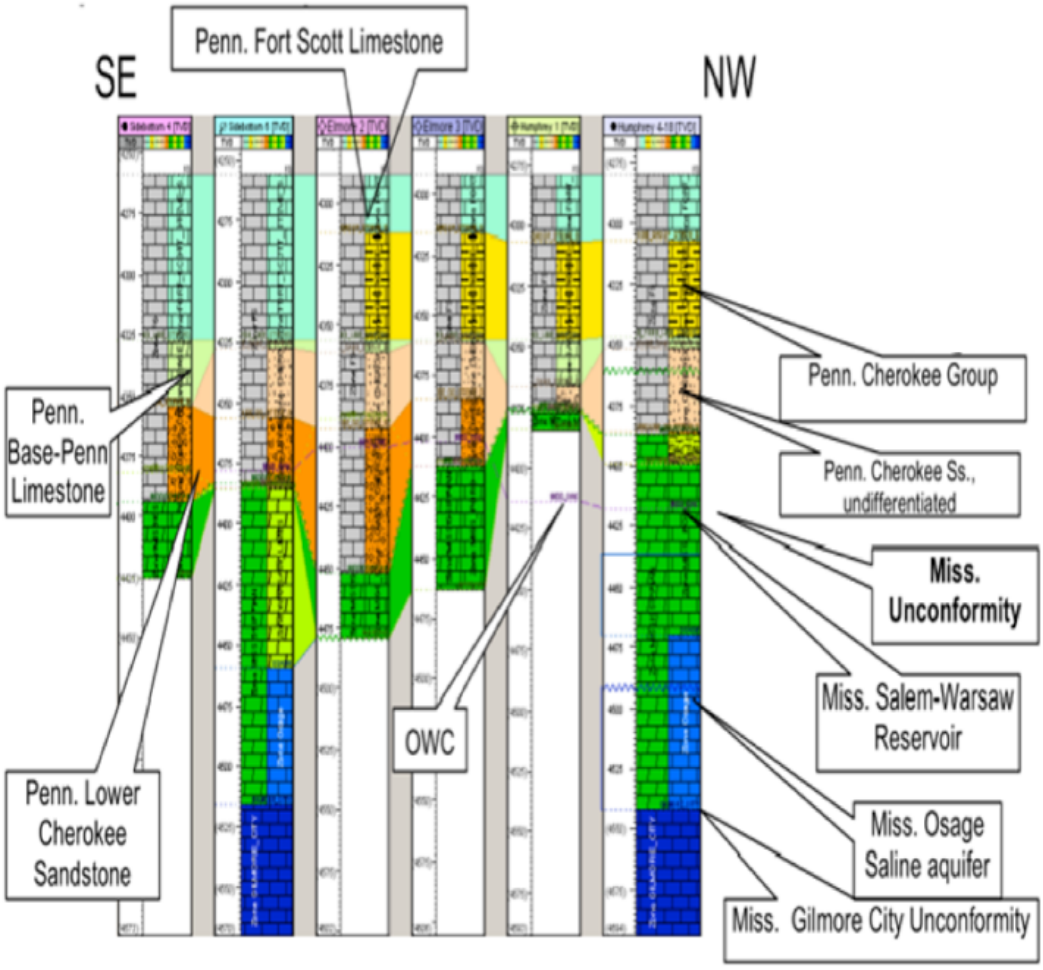

Figure 1.3: Lithologic cross section showing geological formations from top to bottom (Liner 2009)

Well name	Inline number	Crossline number	Density log	Sonic log	Porosity log
Humphrey 4-18	91	59	X	X	X
Dickman 1	119	97		X	X
Dickman 6	103	110		X	X
Elmore 3	71	86		X	X

Table 1.1 Available wells and their logs used in this study

Chapter 2: Pre-stack Seismic Inversion

2.1 Introduction

The goal of pre-stack seismic inversion is to estimate P-impedance (Zp), shear-impedance (Zs), density (ρ) and Vp/Vs from seismic reflection data. It takes advantage of the angle-dependent amplitude and phase variations at each Common Mid Point (CMP) location (Appendix A). Until recently, pre-stack inversion was considered a high cost operation due to the large processing time and computer resources requirements. However, with the advancement of computer technology, this approach is becoming increasingly popular. Although we wish to estimate pseudo-logs from seismic data, the information content of the inversion results is generally limited by the bandwidth of seismic recording which is far below the vertical resolution of a well log. To overcome this, I employ the Very Fast Simulated Annealing algorithm (Srivastava and Sen 2010), which is a global optimization method that searches for a minimum of the objective function that measures data misfit and honors the statistics derived from well logs. This algorithm uses a fractional Gaussian distribution algorithm to generate starting models for VFSA inversion using logs derived from extrapolating away from and interpolating in between available well logs. The results are the inverted volumes of elastic properties with broader frequency content than obtained by a conventional deterministic inversion approach.

The procedure to perform VFSA pre-stack seismic inversion is described in Table 2.1. As a standard procedure, I first tie well logs with post-stack seismic data using synthetic seismograms at the well locations. Different wavelets are then extracted from the tied well logs. This is followed by conversion of NMO corrected pre-stack offset

gathers to angle gathers. Pre-stack inversion of angle gathers is carried out in which forward modeling is done using a linearized Zeopritzz equation. The inversion algorithm estimates compressional (Zp) and shear impedances (Zs), and their associated uncertainty values.

2.2 Data Preparation

2.2.1 Generation of Angle Gather

The input data is a 3D seismic volume that has been fully processed and Normal Move-Out (NMO) corrected (Figure 2.1). Since the inversion algorithm uses seismograms in the angle domain, I convert all of my gathers from offset domain to angle domain, in which the offset of a point is the angle that incident ray comes to that point (Todd and Backus, 1985; Resnick, 1993). Due to the depth to the target (about 4800ft-5500ft) and the maximum offset of 6000ft, the maximum incident angle at the target is approximately 45^o. However, due to the poor quality of seismic data at far offset, I limit the angle range to 30^o. Therefore, the angle-gather ranges from 0^o to 30^o with increment of 5^o for each angle group.

The conversion algorithm requires a velocity model to convert from time to depth, which is then used for angle calculations. In the angle domain seismic gather, traces within the same angle group are summed up and normalized; the resulting trace is used as a representative trace for that angle range (Figure 2.4).

2.2.2 Starting Models

I construct starting models for three model parameters – P-impedance (Zp), S-impedance (Zs) and density (ρ) using simple interpolation between well logs that have been tied with seismic data and extrapolation away from well logs. The interpolation and

extrapolation is guided by horizons that are picked from the seismic volume (Figure 2.5). At each CMP location, the pseudo-log is used to derive fractal parameters. Figure 2.6 shows an example of fractal models of Zp, Zs and Density at a particular well location compared with the common low frequency starting model.

The purpose of creating a fractal-based model is to improve the frequency content of the inversion results by introducing fractal contents of starting model. Appendix A describes the details of the algorithm that generates this starting model. In brief, the process calculates statistical parameters of input models (Zp, Zs and density) such as mean, standard deviation and Hurst coefficients (Hurst 1951). Given these three parameters at a CMP location, a starting model is drawn from a fractional Gaussian distribution, which is used in the seismic inversion.

2.2.3 Shear and Density Logs

The well log data are used as constraints in the inversion process. It requires density, sonic and shear logs to calculate P- and S-impedance data. However, since only well Humphrey 4-18 contains density and sonic logs, while the other three wells contain only sonic log, I first estimate density from sonic logs using a known mathematical formula given by Gardner (1974).

I assume that the density of the target formation does not vary spatially significantly in the Dickman Field. Since this is a carbonate reservoir, I am using Gardner's equation (Gardner 1974- Equation 2.1) to calculate bulk density from P-wave velocity, which can be obtained from sonic logs. The Gardner's equation is commonly used to calculate density from sonic log in case density log is not available. The equation is applicable for sedimentary rocks (sandstones, carbonates, shale) from a wide variety of

basins and depths (Miller et al 1991). I also employ Lindseth's equation (Lindseth 1979-Equation 1), which is an alternative to Gardner's equation:

$$\rho = 0.23V_p^{0.25} \quad Gardner's\ Equation$$
$$\rho = \frac{V_p - 3460}{0.308V_p} \quad Lindseth's Equation \qquad (2.1)$$

Where density ρ is in g/cc and velocity Vp is in ft/s. To examine the quality of the conversion, I plot density results from Equation 2.1 at well Humphrey 4-18 (Figure 2.2). Both equations from Equation 2.1 give excellent fits to real density logs, but Gardner's result provides slightly better fit. Therefore, I use Gardner's equation to generate density logs at three other wells.

Shear log is another required log for pre-stack seismic inversion. There are no available logs of this type in all wells. I use Castagna's equation (Castagna 1985)-(Equation 2.2) to generate shear wave velocity from P wave velocity, assuming the formation is 100% water saturated.

$$Vs = 0.8621\ \text{Vp} - 3846.8 \text{ (Units: ft/s)} \quad (2.2)$$

2.2.4 Well Tie and Wavelet Estimations

It is critical that well log is tied with seismic data, since our analysis uses well logs as constraints for quality control. To perform well tie, I display the well and horizon picks (in time domain) together with post-stack seismic data. By matching the horizon tops reported in the data set at the well and the horizons already picked, I can match the well log with seismic data. The process is carried-out for a small target interval from 700ms- 910ms since I assume the wavelet does not change its properties (frequency content and amplitude) within that target interval. The well tie is done by computing post-stack synthetic seismograms based on the well log and modifying the well log

slightly so that the reflection events in the synthetic correlate well with those in the data. The result is a new set of well logs that are in time domain and ready for further analysis. An example of well logs of well Humphrey 4-18 tied successfully with seismic data is in Figure 2.3.

Wavelet estimation is a mathematical process in which wavelets are estimated from the seismic data at the well locations. A seismic trace at a particular well location is extracted from seismic data. This seismic trace is the product of a convolution between a wavelet and a reflectivity series. That is,

$$Rpp = \frac{\rho_2 vp_2 - \rho_1 vp_1}{\rho_2 vp_2 + \rho_1 vp_1} \qquad (2.3)$$
$$Rpp * wavelet = seismic\,traces$$

where '*' represents a convolution. The reflectivity Rpp is calculated from well logs that have been tied and converted from depth to time domain using P-wave velocity and density logs. Meanwhile, the wavelet is estimated by solving Equation 2.3 with known values of Rpp and seismic traces. The results are three wavelets corresponding to three different angle ranges of 0^o-10^o, 11^o-20^o and 21^o-30^o.

2.3 Inversion Results

The inversion algorithm generally converges in 800 iterations for each Common Mid Point (CMP) location. The input decay factor is set to be 0.45, maximum number of random moves per iteration is 3, the number of trial at each move is 25, the starting temperature is 100^o, and the model temperature is set to be 2.0^o. Figure 2.7 shows the inversion results of P-impedance, S-impedance and density at a well location. Note that the results of inverted Zp and Zs are close to the original log, while the result of density is not matching. The difference between synthetic angle gather and real angle gather is

small for near angle, and larger at high angle (Figure 2.8). The overall error decreases to a limit where no further accuracy can be achieved (Figure 2.9). The error reaches a stable level where more iteration does not improve inversion results significantly after 700 iterations.

Figure 2.10 shows the inverted impedances on top of Mississippian carbonate formation. The average impedance is about 45000 g/cc* ft/s for Zp, and 32000 g/cc*ft/s for Zs. Comparing the results with those from starting models, the inversion does improve the visibility of impedances (both Zp and Zs) at the South West corner of the field. Meanwhile, at the Northwestern part of the field, inverted impedances are fairly uniformly distributed.

2.4. Summary

I successfully invert seismic data to obtain impedance (Zp and Zs impedance) and density values for the whole 3D cube. The inverted results of Zp and Zs match well with original well logs. The introduction of fractal based starting model improves the resolution of impedance patterns at the South West corner of the field. Meanwhile, obtained density does not match well with well log data. There are many reasons for density mismatch. First, the original angle gather is limited to a maximum angle of 30 degrees. The linearized Zeoppritzz equation (Appendix A) employed as a forward modeling for inversion process requires larger angle value so that the density contrast term ($\Delta\rho/\rho$) can have influence on the reflection coefficient. Secondly, looking closely at original angle gathers, the seismic data contains lots of noise that prevent the inversion process to be more accurate.

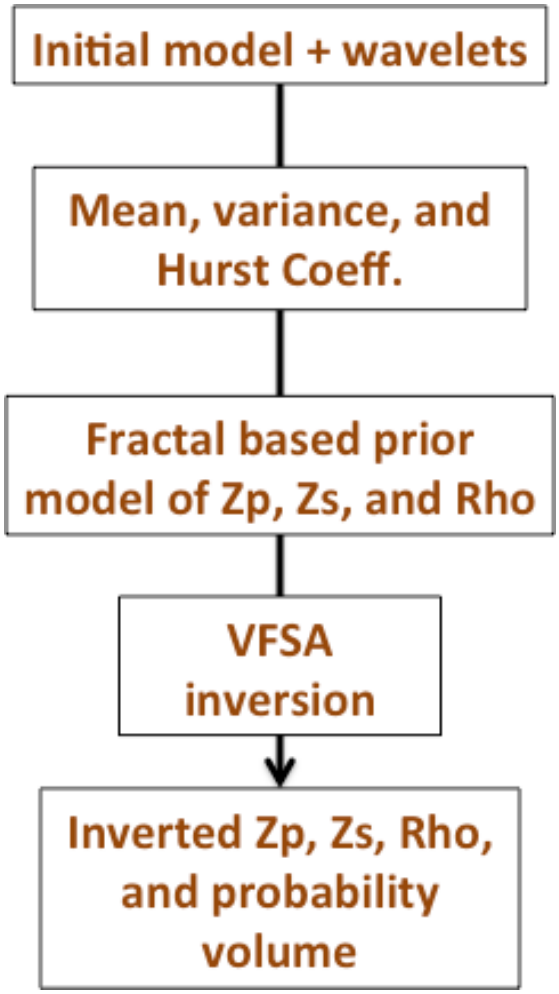

Table 2.1: Work flow of a VFSA inversion from Srivastava and Sen 2010

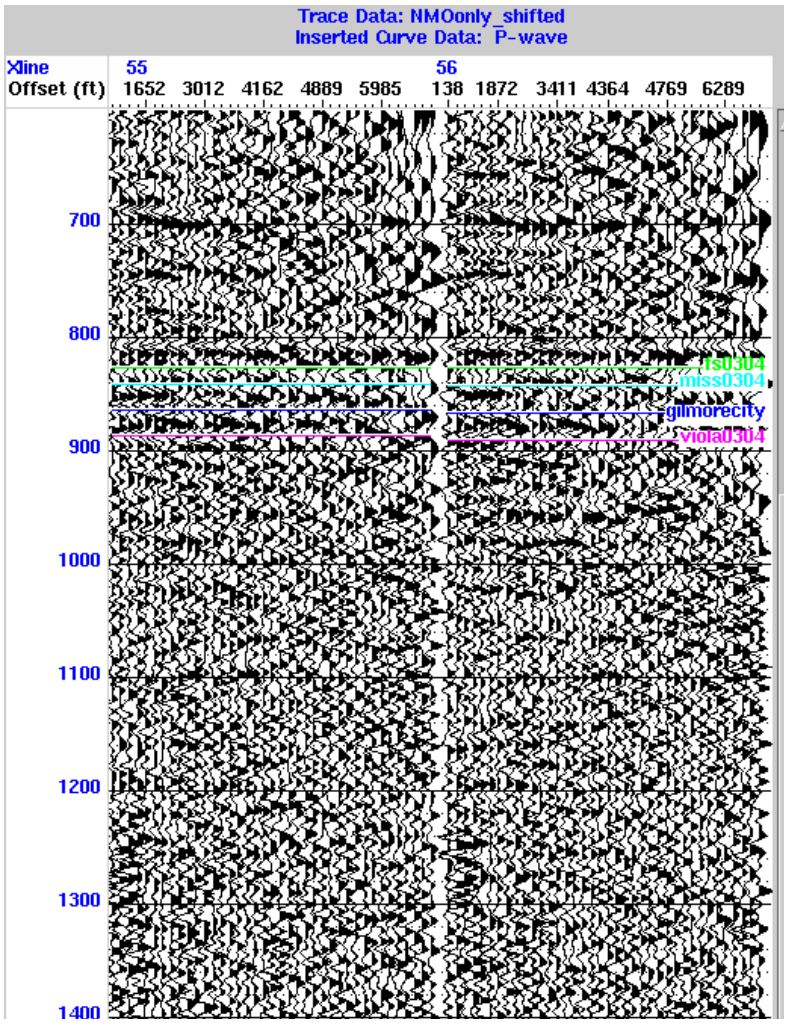

Figure 2.1: Pre-stack NMO corrected seismic data at two CMP locations

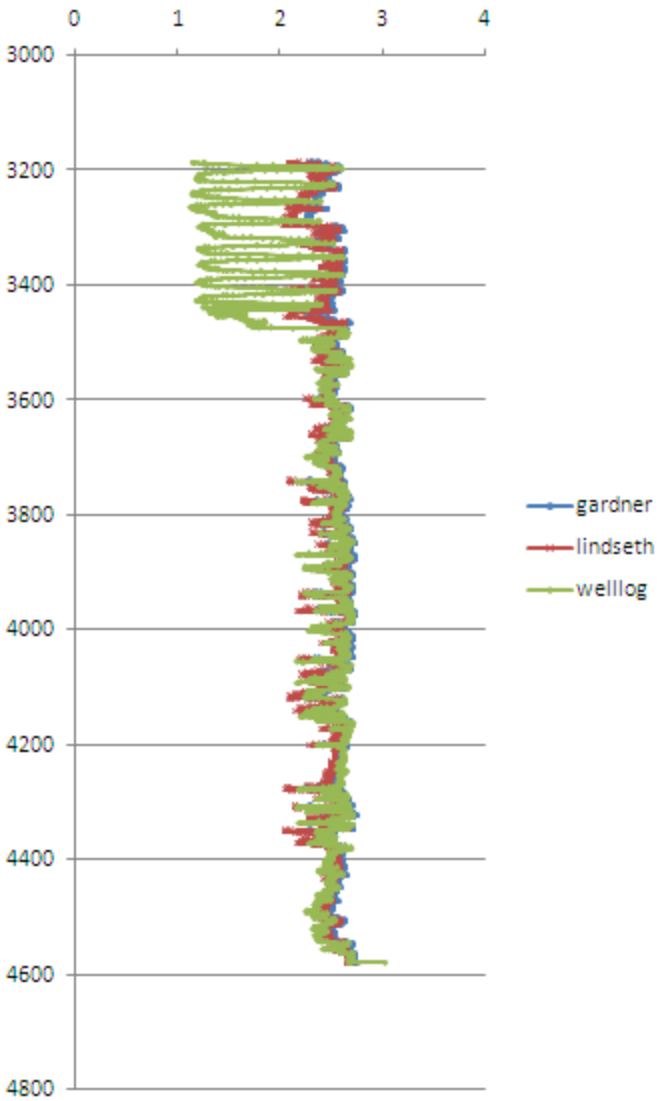

Figure 2.2: Density generated from Gardner's and Lindseth's equations plotted against density from well log at Humphrey 4-18. Result from Gardner's equation is closer to real log and therefore is used for further investigation.

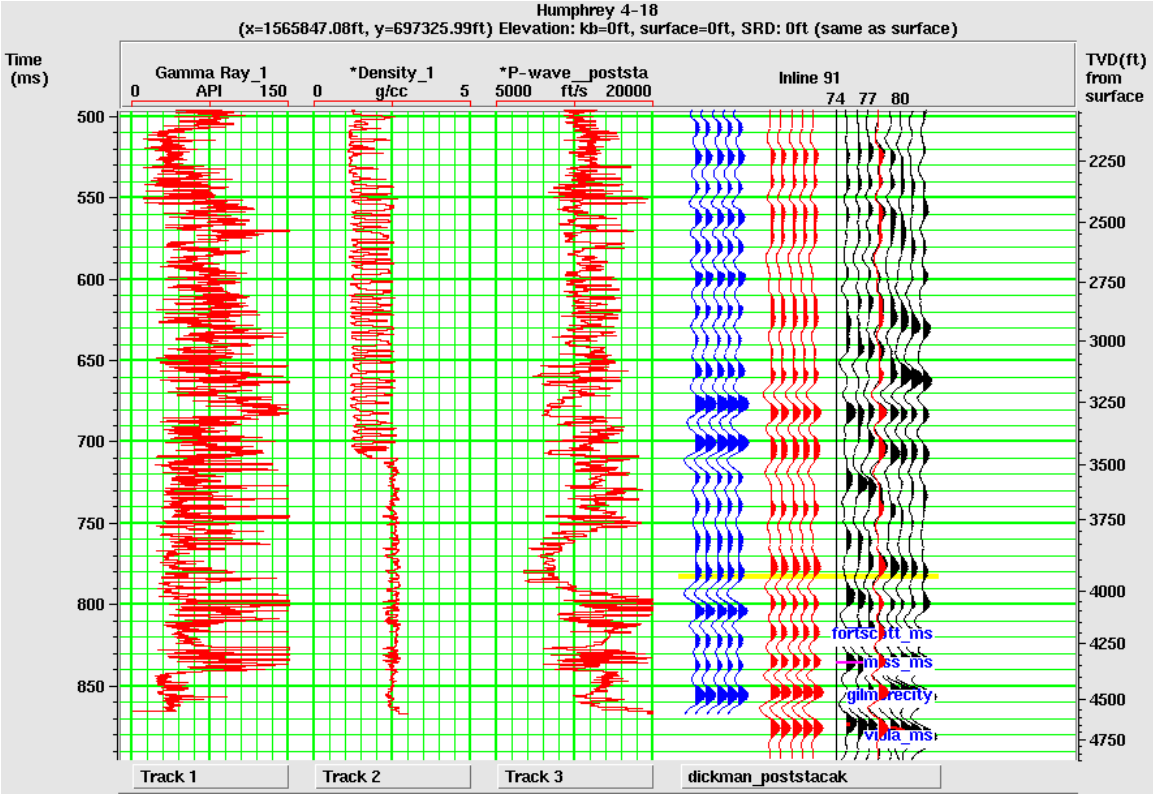

Figure 2.3: well tie performed at Humphrey 4-18 showing good correlations between synthetic traces (blue) and real seismic data (red)

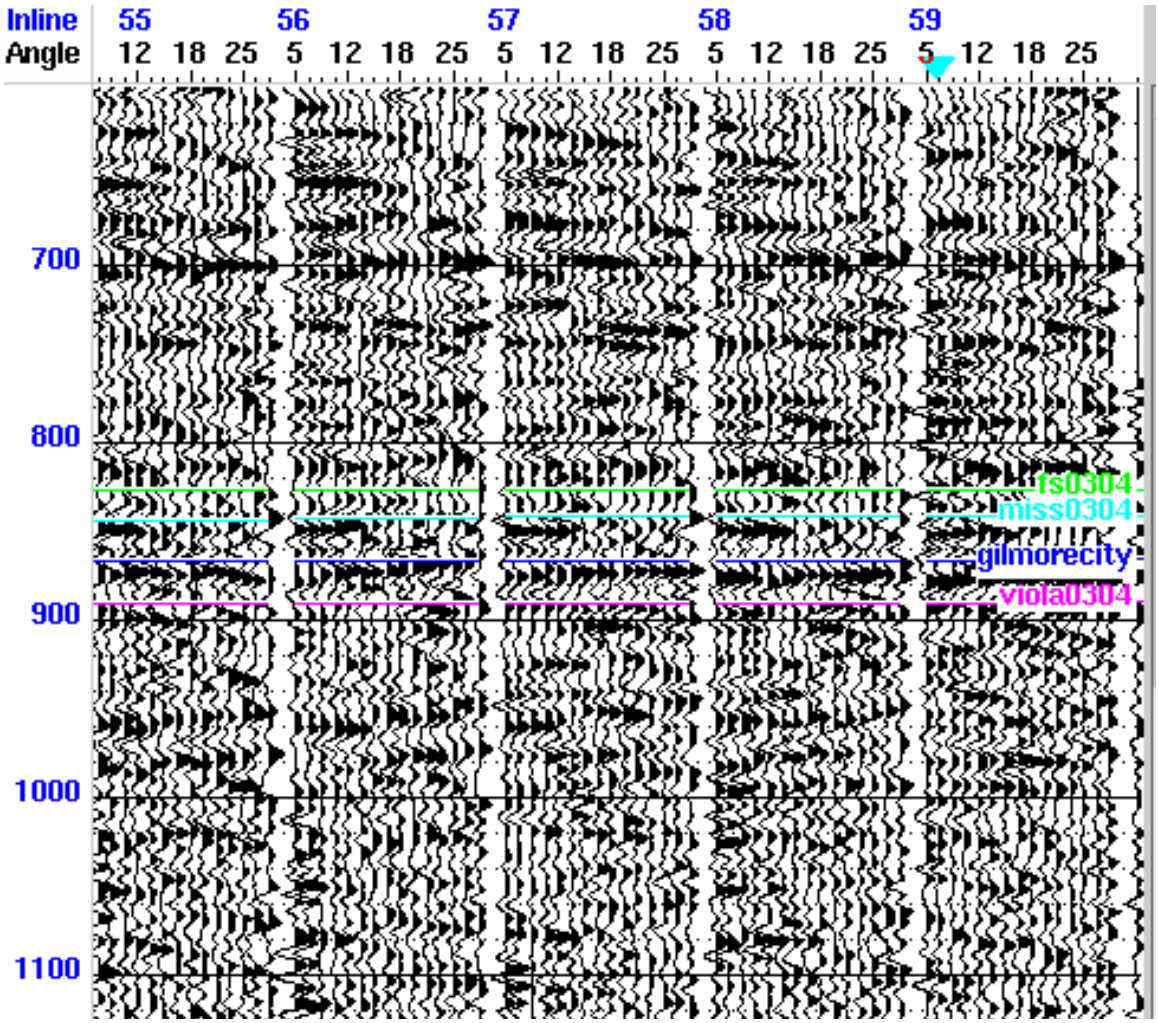

Figure 2.4: Angle gathers at five CMP locations: the angle ranges from 0 to 30 degrees

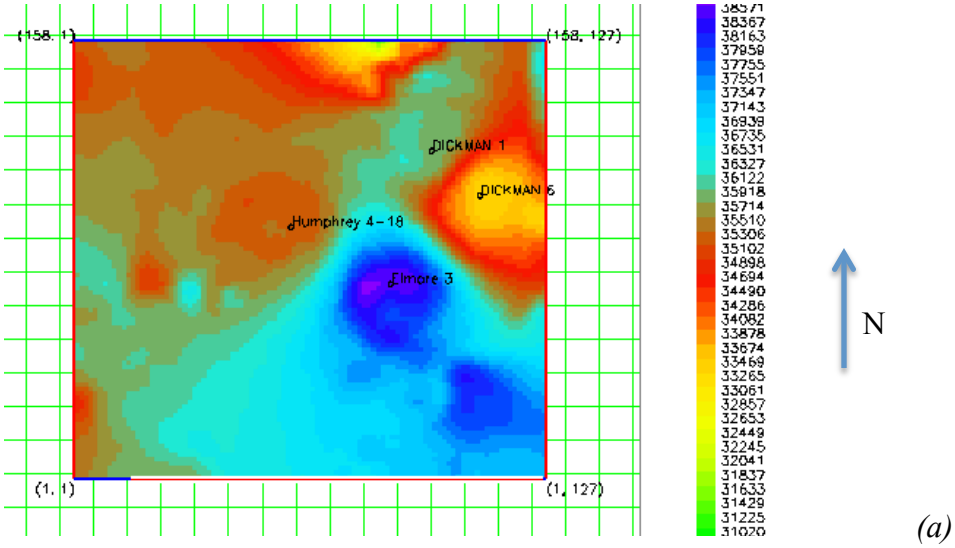

(a)

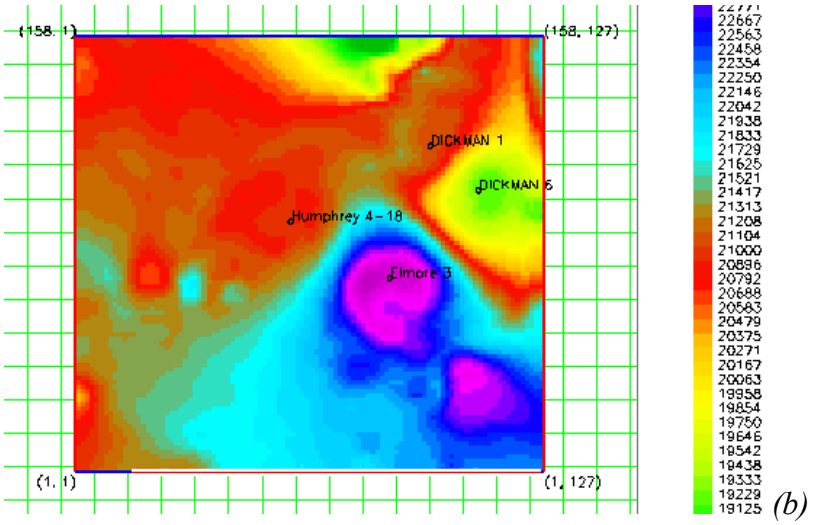

(b)

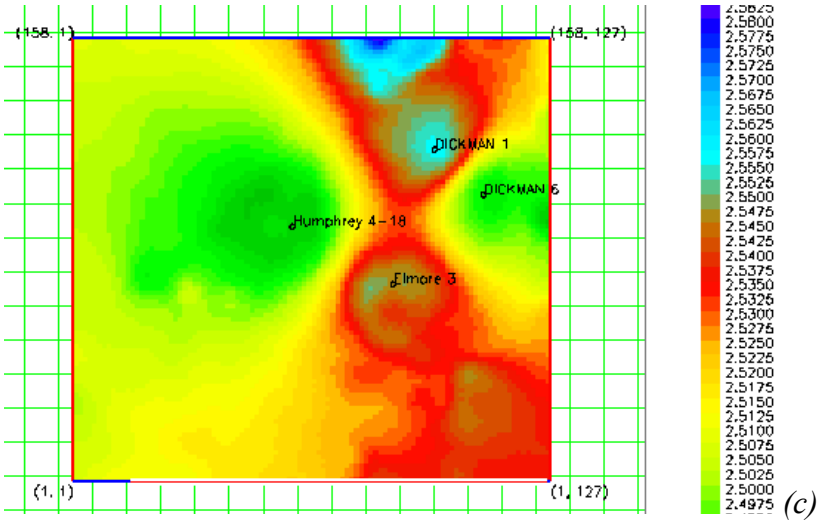

(c)

Figure 2.5: A horizontal slice of Starting models of (a) Zp, (b) Zs, (c) Density on top of Mississippian Carbonate

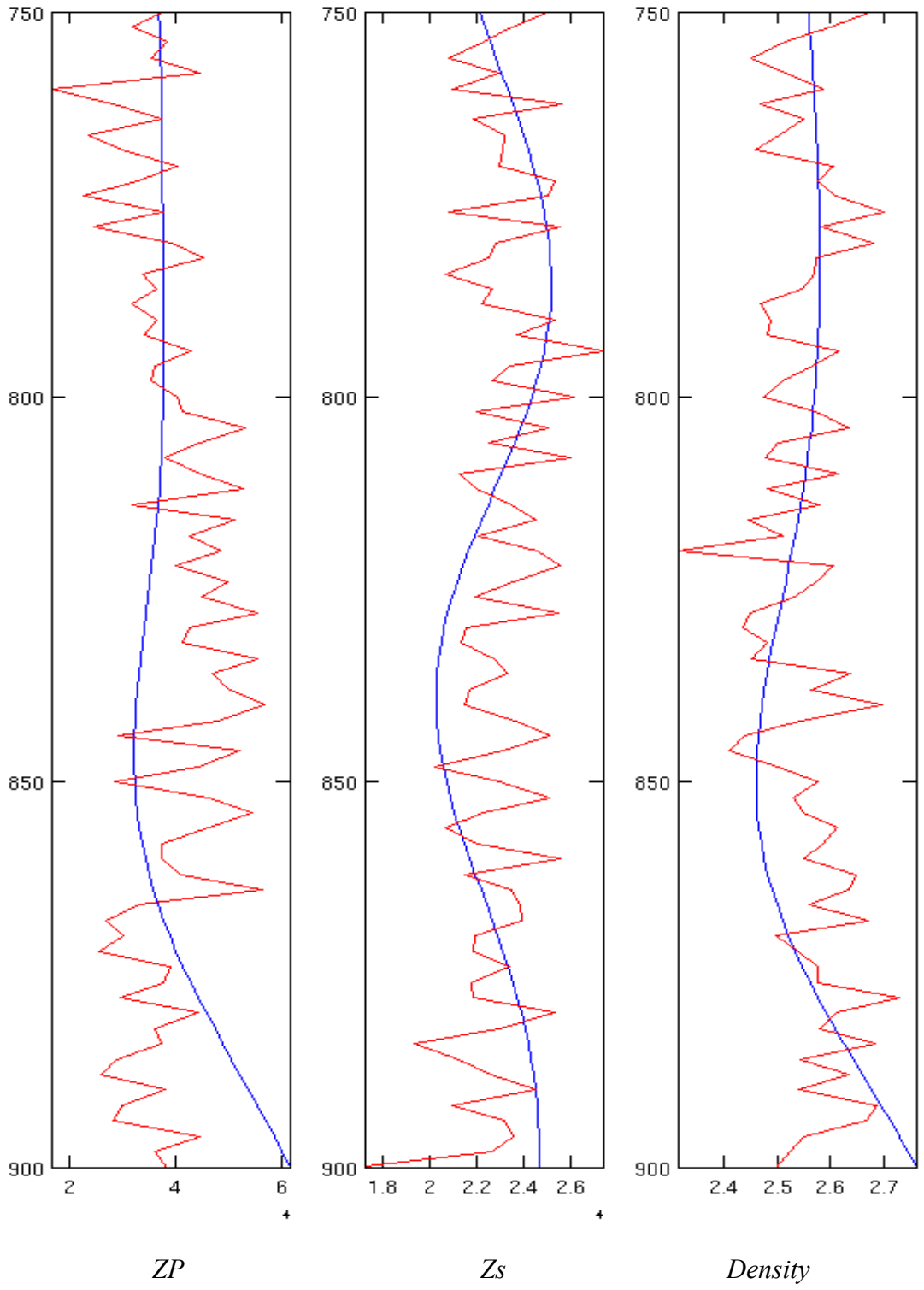

Figure 2.6: An example of fractal based initial model (black) compared with the conventional smooth low frequency starting model (red).

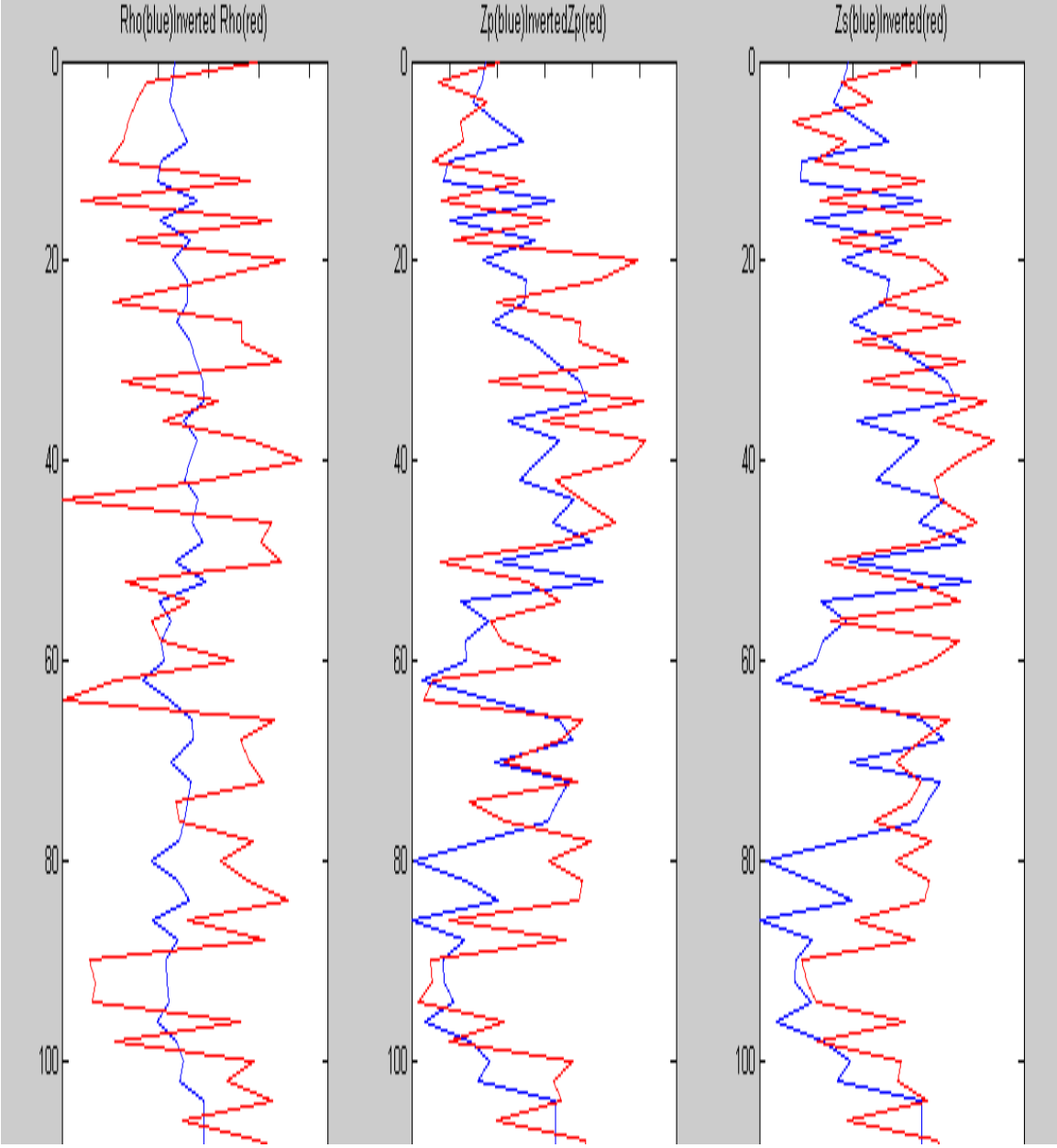

Figure 2.7: seismic inversion result at a well location. The red curves are the inversion results, and the blue curves are original los at the well location. Note that the Zp and Zs match very well but the density estimates are not accurate.

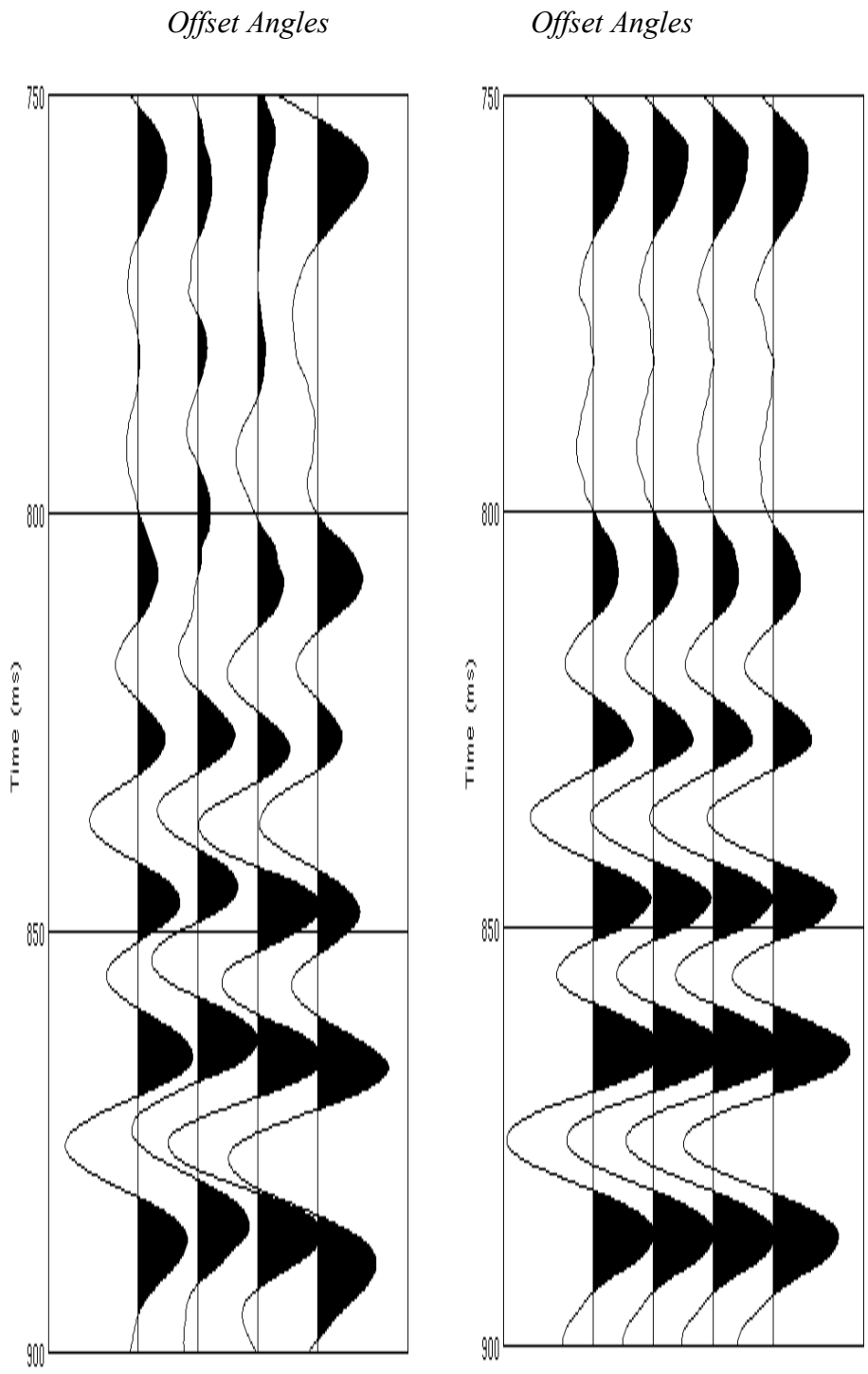

(a) Real gather *(b) Synthetic Gather*

Figure 2.8: (a) Angle gather at well Humphrey 4-18 location, (b) synthetic angle gather generated from inverted results

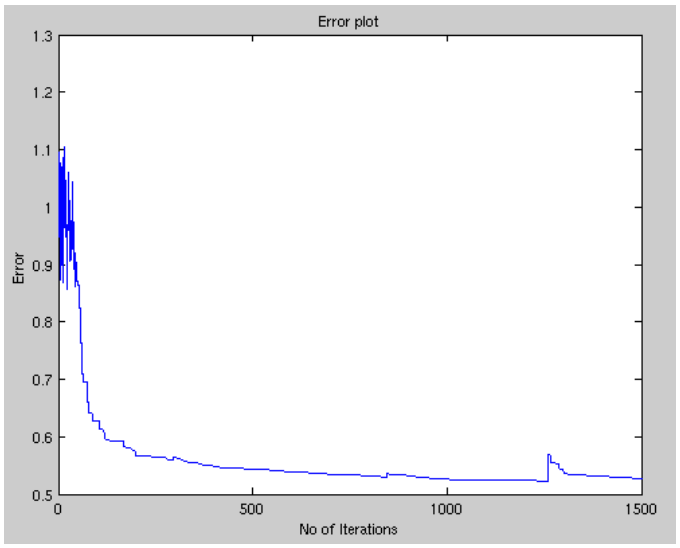

Figure 2.9: Objective function in VFSA inversion

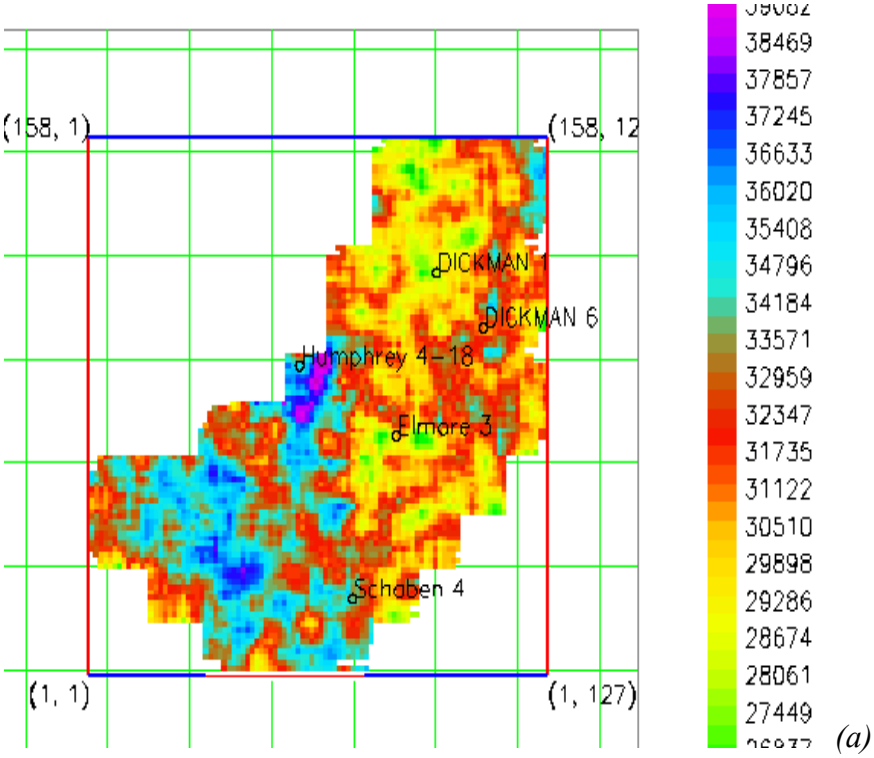

(a)

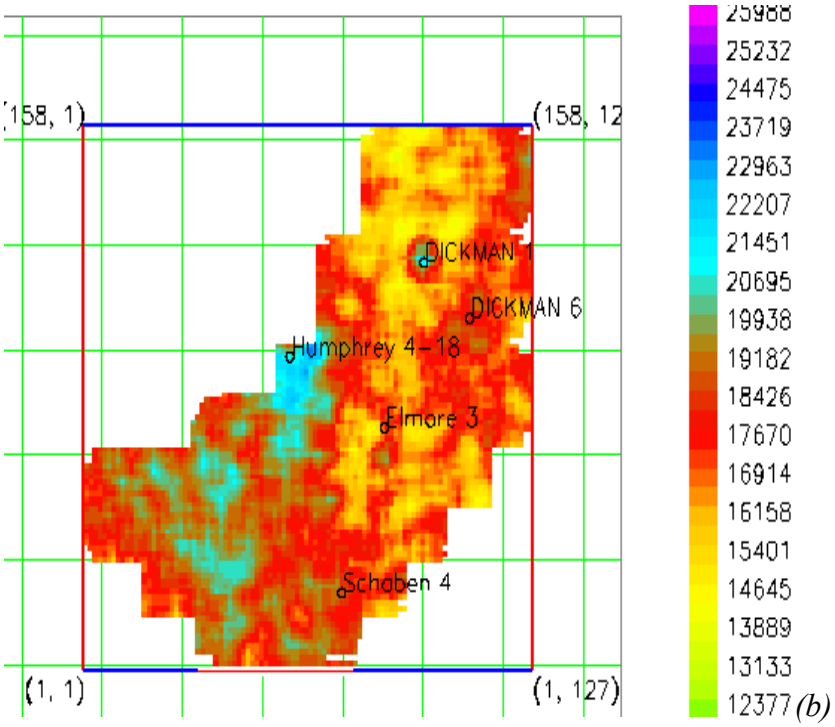

*Figure 2.10: Impedance slices along the top of Mississippian Carbonate from pre-stack seismic inversion: (a) Inverted Zp, (b) Inverted Zs. The color bar unit is in (ft/s*g/cc)*

Chapter 3: Reservoir Parameter Estimation

3.1 Introduction

In this chapter, I describe a procedure for estimating porosity and permeability of the model between 750ms and 900ms below the surface using the inverted results from pre-stack seismic inversion. Porosity is generally estimated from seismic impedances. There are several approaches to doing this, which include geo-statistical data integration (Angeleri et al 1982, Doyen 1988), and multi-attribute regression analysis (Schultz et at 1994, Hampson et al 2001- Figure 3.0). For this study, I use a multi-attribute regression analysis method. The objective of this method is to derive a multi-attribute transform, which is a linear or non-linear transform between a subset of the attributes (in my case, they are the inverted volumes) and the target log values (porosity logs at well locations). In linear mode, the transform consists of weights derived by least-squares minimization. In the non-linear mode, a neural network is trained using the selected attributes as inputs (Hampson 2001). For quality control, final results (porosity) are plotted against real log data (porosity log) at the well locations.

Permeability is an essential parameter in flow simulation. A common method to estimate it is by establishing a functional relationship between this parameter and porosity for the same rock type. Since I assume that the permeability-porosity relationship of the Mississippian Carbonate does not change throughout the research area, this method is reasonable.

3.2 Porosity Estimation

All the four wells used for this study contain neutron porosity log. The input models for porosity estimation are the inverted results from seismic inversion, namely

Zp, Zs and density. The Vp/Vs is obtained simply by taking the ratio between Zp and Zs. The post-stack seismic data is also used as a valid input, since the porosity does have effect on the seismic amplitude.

The correlation between a single attribute and porosity is very low (in Figure 3.1, the maximum correlation is 0.39 for Zs and porosity). The purpose of introducing a multi-attributes analysis is to overcome the low correlation between a single attribute of an input model and porosity. The chart in Table 3.1 displays the workflow of this step.

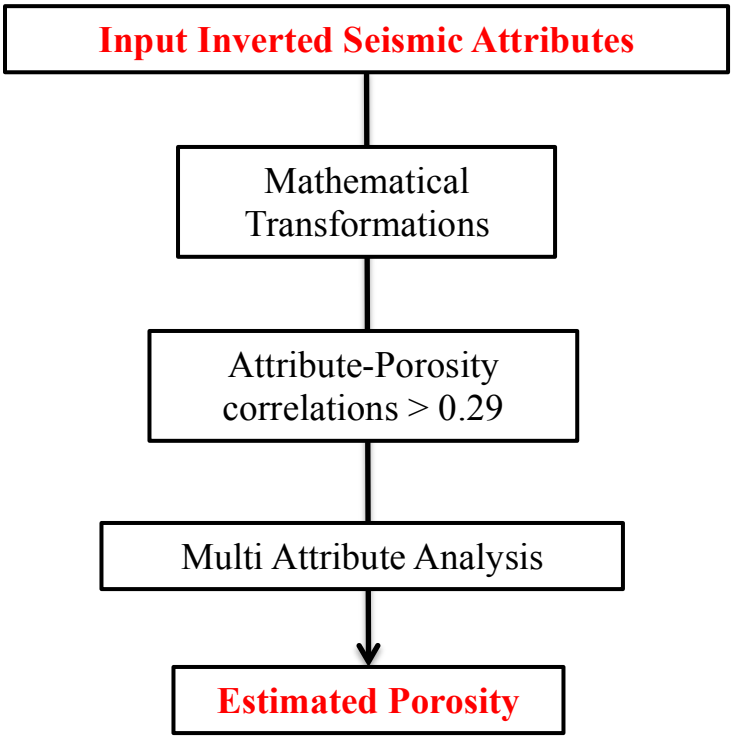

(Table 3.1)

3.2.1 Multi-attribute Analysis

Multi-attribute analysis is the extension of the linear analysis to include multiple input attributes to the algorithm. This mathematical approach is discussed in great detail in Hampson et al (2001). I summarize this approach here, for completeness. The target log L(t) is modeled by an equation which is a linear combination of input attributes $A_i(t)$

with different weights w_i. The assumption for this case is that each attribute is associated with a single weight, which is:

$$L(t) = w_0 + \Sigma\, w_i\, A_i(t);\ i = 1, 2, \ldots n \quad (3.1)$$

where n is the number of input attributes. The weights w_i's are calculated by minimize a L2 norm error function calculated from target log L_i:

$$E^2 = 1/N * \Sigma\, (L_i - w_i\, A_i(t))^2 \quad (3.2)$$

From the error function, assuming there are n input attributes, there are n+1 weight values w's to be estimated. The solution for n + 1 weights is expressed as:

$$\begin{bmatrix} w0 \\ w1 \\ . \\ . \\ wn \end{bmatrix} = \begin{bmatrix} N & \sum A_{1i} & \sum A_{2i} & \ldots & \sum A_{ni} \\ \sum A_{1i} & \sum A_{1i}^2 & \sum A_{1i}\sum A_{2i} & \ldots & \sum A_{1i}\sum A_{ni} \\ \sum A_{2i} & \sum A_{1i}\sum A_{2i} & \sum A_{2i}^2 & \ldots & \sum A_{2i}\sum A_{ni} \\ . & . & . & .. & . \\ \sum A_{ni} & \sum A_{ni}\sum A_{1i} & \sum A_{ni}\sum A_{2i} & \ldots & \sum A_{ni}^2 \end{bmatrix}^{-1} \cdot \begin{bmatrix} \sum L_i \\ \sum A_{1i}L_i \\ \sum A_{2i}L_i \\ . \\ \sum A_{ni}L_i \end{bmatrix} \quad (3.3)$$

However, the assumption on a single weight is not valid as the target log is frequency dependent. The frequency content of the target log is usually higher than that of the seismic attributes. To overcome this, the assumption is modified such that each sample of the target log is related to a group of neighboring samples on the seismic attributes. This suggests employing a convolution operator in which a group of consecutive points from the attributes are used to estimate a single point on the target. Figure 3.0 shows an example of the 5-point convolution operator to relate seismic attribute to target log (Hampson et al 2001). The length of the convolution operator is the number of neighboring samples that are used. With this convention, the target log is slightly modified to include the convolution operator. For this data set, I used an operator

length of 7. According to Hampson et al (2001), the attributes that carry porosity correlations of less than 0.29 will not have noticeable distributions to the final predicted result. This is an important criterion that I follow to choose the attributes as it helps limiting the number of available attributes. Below is a list of 13 attributes that I use to predict porosity from multi-attribute analysis:

1. *Zp*
2. *1/Zs*
3. *1/(Vp/Vs)*
4. *Filter 35/40 -45/50*
5. *Amplitude Weighted Phase*
6. *Amplitude Weighted Cosine Phase*
7. *Derivative Instantaneous Amplitude*
8. *1/Density*
9. *Filter 12/20 – 25/30*
10. *1/Vs*
11. *Instantaneous Phase*
12. *Instantaneous Frequency*
13. *Apparent Polarity*

3.2.2 Estimated Porosity

The neutron logs at the well locations are used to constrain porosity results. Liner et al (2009) reported the porosity on top of Mississippian Carbonate to range from 8% to 25%, with an average of 21%.

I obtain high correlation between predicted porosity at the well locations and the real porosity logs. At well locations (Figure 3.5), the error is of 1.65% and the correlation value is 0.968. The histogram of porosity values along the Mississippian Carbonate top (Figure 3.6 (a)) shows that the porosity ranges from 7.5% to 25%, with an average of 18%. This is close to the range reported in Liner (2009) report. From Figure 3.6 (b), most high porosity zones are near Dickman 1 and Dickman 6 wells. The lowest porosity is in the vicinity around Humphrey 4-18, which is at the edge of the seismic volume.

3.3 Permeability Estimation

I applied Timur (1968) equation that shows a relationship between permeability k and porosity phi (Φ). The relationship is expressed as

$$k = 0.136 \frac{\Phi^{4.4}}{S_{wir}{}^{2}}, \qquad (3.4)$$

where S_{wir} is irreducible water saturation in unit of percentage, and is assumed to be 20%. Porosity Φ is obtained from porosity estimation process above and has the unit of percentage, permeability k with unit of milli-darcys. The primary permeability calculated from Timur's equation is displayed in Figure 3.2.

Primary analysis on the distribution of porosity in the Mississippian Carbonate shows that there are three different rock classes corresponding to three porosity group of values: low porosity (7.5-12%), medium porosity (12-21%) and high porosity (21-29%) (Figure 3.3a). The second group is the dominant one which most of the values are in. With this observation, after an initial permeability has been estimated, I try to classify rocks into different classes using Winland R35 method (published by Kolodzie (1980)). I assume that rocks of the same class share similar properties. Since there has been no

effective unique mathematical relationship to express the connection between those two parameters, it is not reliable to correlate using just Timur (1968) equation above.

By using Winland R35 to classify rock classes, I will process correlation using rock classes, which is more logical. Winland R35 equation, which is,

$$Log\ (R35) = 0.732 + 0.588\ Log\ (K) - 0.864\ Log\ (\Phi), \quad (3.5)$$

where R35 (μm) is the pore throat radius corresponding to the 35th percentile mercury saturation, k (md) is permeability and ϕ (percentage) is porosity. The permeability values calculated from Timur (1968) (Figure 3.2) is input into Equation 3.5 to calculate the R35 values at well locations. A histogram of R35 values is useful to determine the dominant values, which are the representatives of different rock classes (Figure 3.3b). There are three classes that I observe, which correspond to pore throats radius of [0.5, 5]; [5,10]; and [10, 20] μm. Four new R35 curves of three different ranges are plotted on the same k-ϕ plot to divide the entire interval into three different rock classes. Within each class, I perform a linear fit between k and ϕ, and use that relationship to calculate the actual permeability of the rock belonging to that particular rock class. The same procedure is carried out for the whole field, and the result is a volume of permeability and rock classes.

Figure 3.7(b) shows the permeability distributions along the top of Mississippian Carbonate. The Dickman 1 and Dickman 6 are within a zone of high permeability of a river channel, while Elmore 3 is located near a low permeability zone. The maximum permeability value along the top of Mississippian Carbonate is at 700 md, and the minimum is at 0, which is distributed sparsely throughout the field.

3.4 Summary

Multi-attribute method used in my study appears to estimate reasonable values of porosity. The calculated values fall within desirable range reported by Liner (2009) in an independent study. There is a noticeable high porosity zone on top of Gilmore formation, which has not been reported at the Dickman Field. In Figure 3.8, there are large areas where the porosity is continuous, especially near Elmore 3 and Dickman 1 and Dickman 6 wells. In addition to that, this Gilmore formation is also a saline aquifer. Proper combination of these properties makes Gilmore an excellent candidate for CO_2 injection.

The estimated permeability from Winland's R35 method does show small differences from that predicted by Timur's equation. That is because my input permeability data is generated using Timur's equation (due to the lack of real permeability data), which is generally used to set up a trend for the permeability- porosity curve. If there are available permeability data, the difference between predicted results from Winland's method and Timur's equation should be noticeable since the final results will be constrained by permeability data.

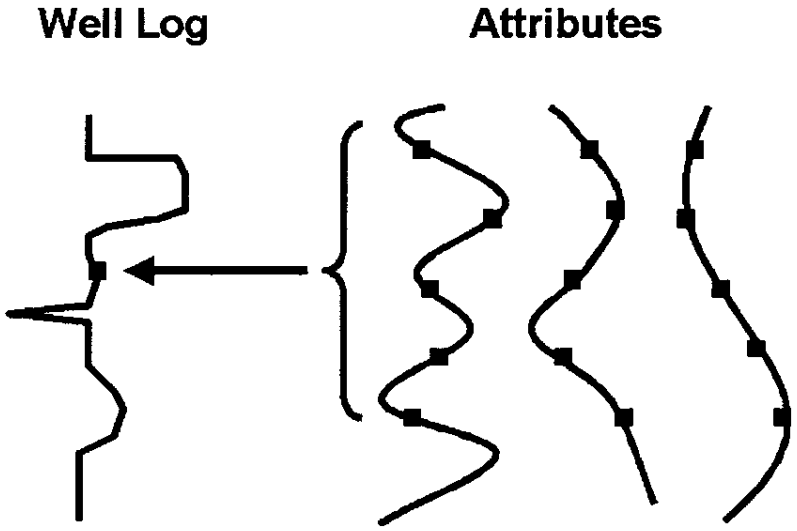

Figure 3.0: The use of 5-point convolution operator to relate seismic attribute to target log (Hampson et al 2001)

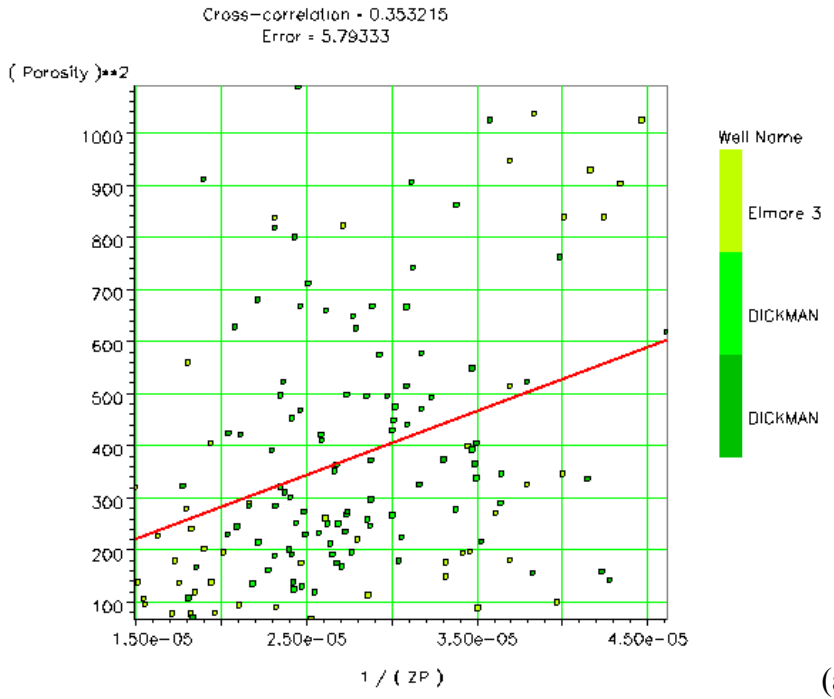
Cross-correlation = 0.353215
Error = 5.79333
(Porosity)**2
1000
900
800
700
600
500
400
300
200
100
1.50e-05
2.50e-05
3.50e-05
4.50e-05
1 / (ZP)
Well Name
Elmore 3
DICKMAN
DICKMAN

(a)

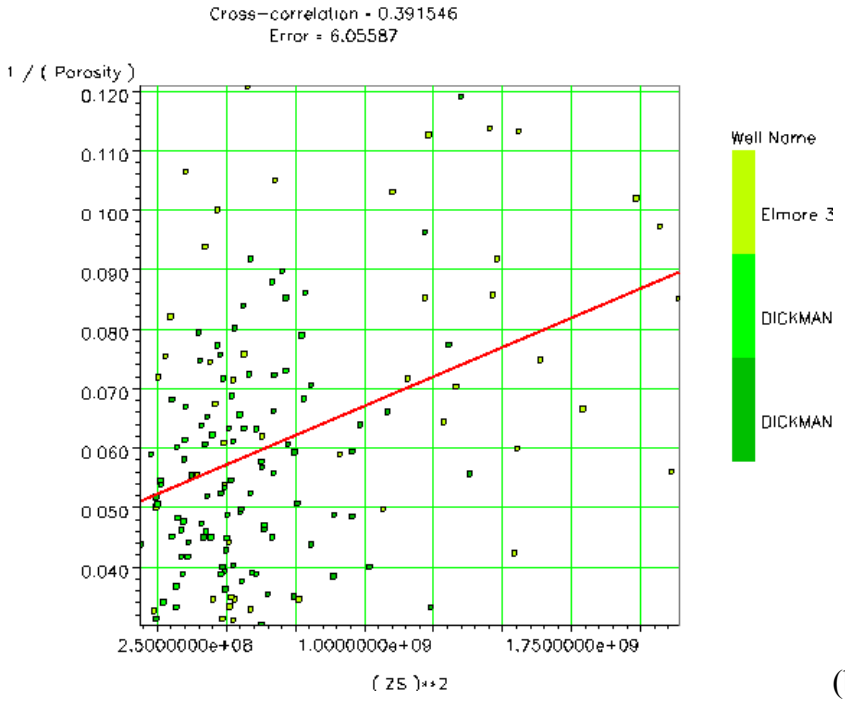
Cross-correlation = 0.391546
Error = 6.05587
1 / (Porosity)
0.120
0.110
0.100
0.090
0.080
0.070
0.060
0.050
0.040
2.5000000e+08
1.0000000e+09
1.7500000e+09
(ZS)**2
Well Name
Elmore 3
DICKMAN
DICKMAN

(b)

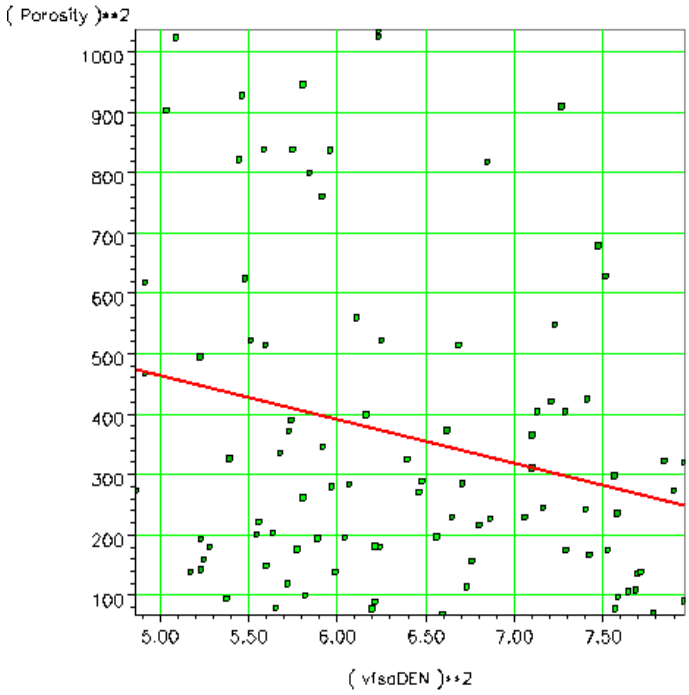

(c)

Figure 3.1: Cross plots showing the correlation between porosity Φ and other parameters (a) Zp, (b) Zs, (c) Density ρ

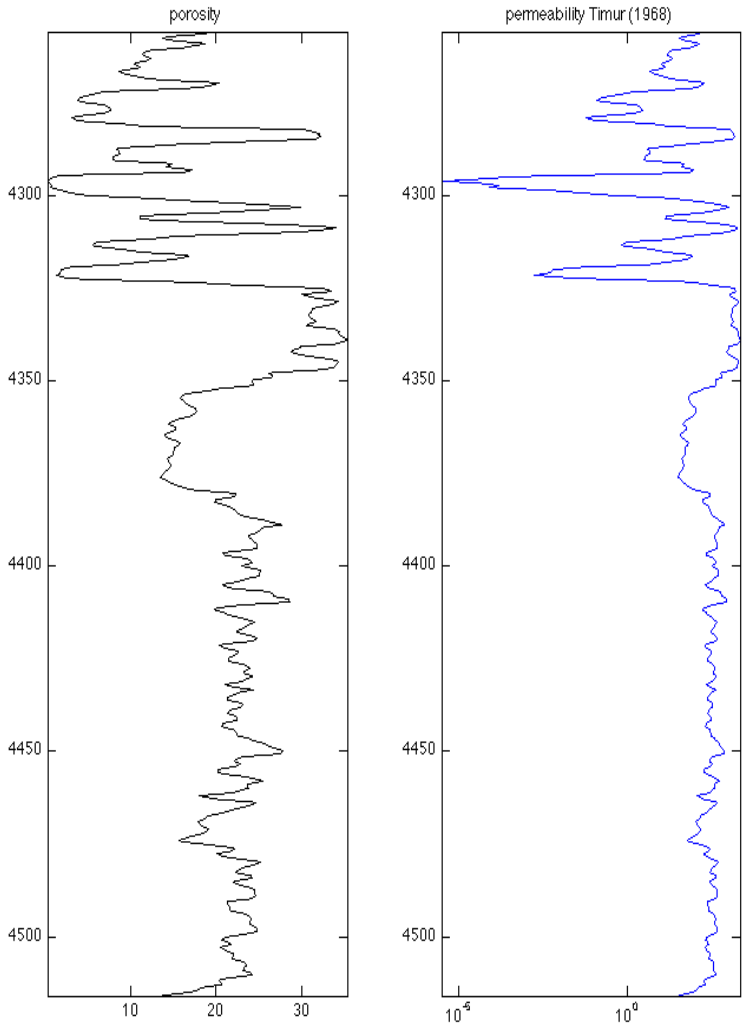

Figure 3.2: Calculated permeability using Timur (1968) equation from corresponding porosity log

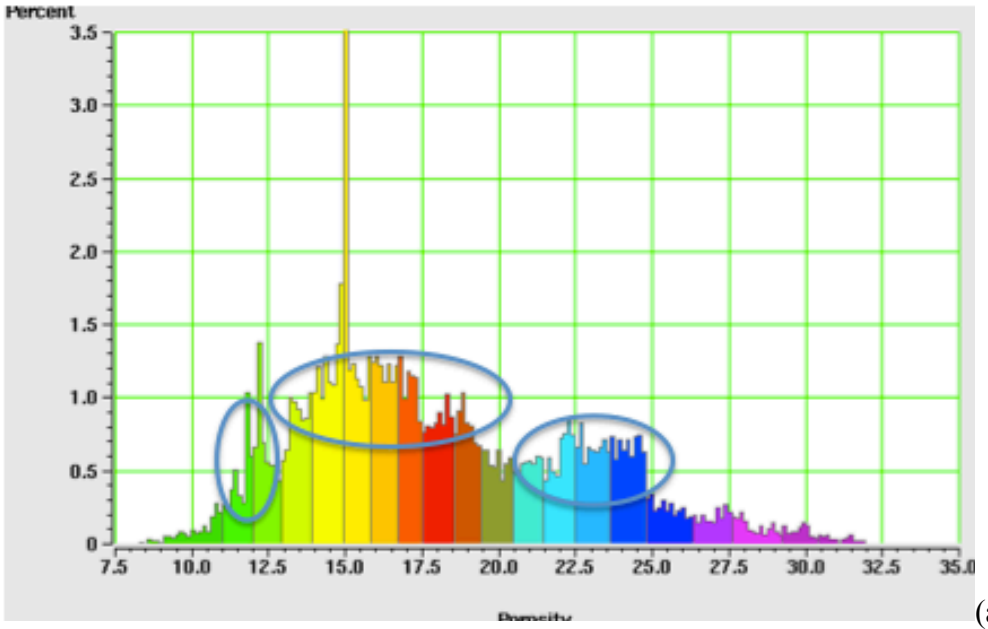

(a)

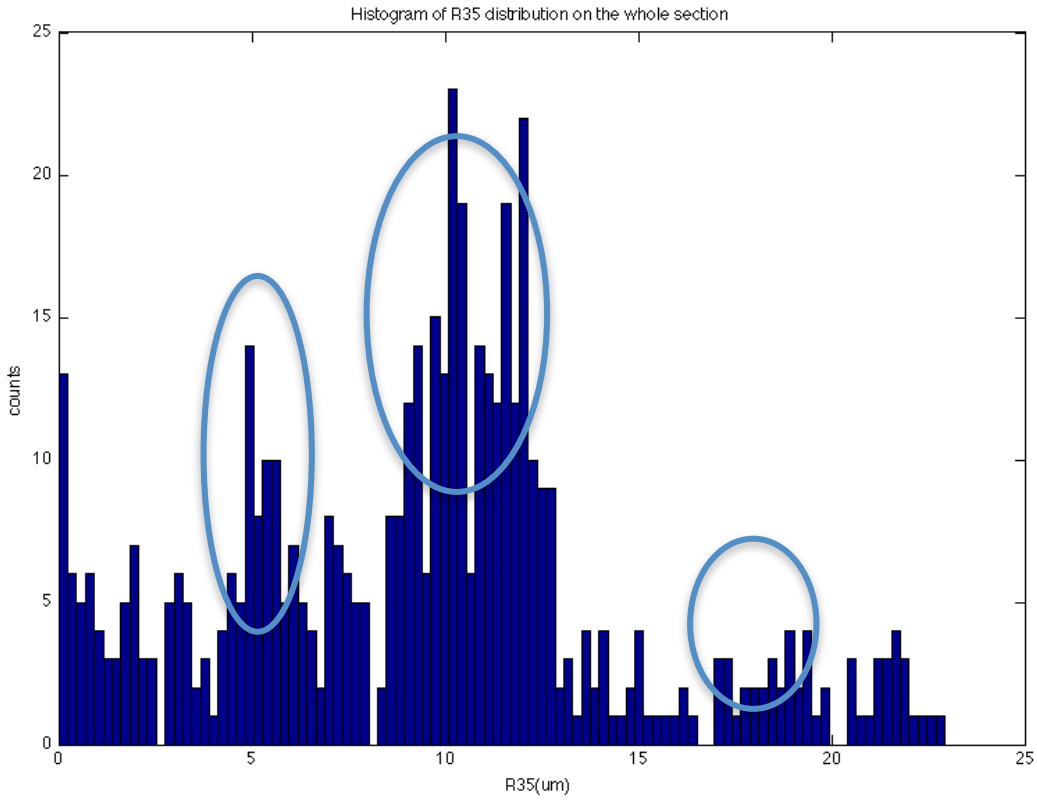

(b)

Figure 3.3: (a) Histogram of Porosity showing three different peaks; (b) Histogram of R35 values shows three dominant R35 values of 5, 10 and 20µm

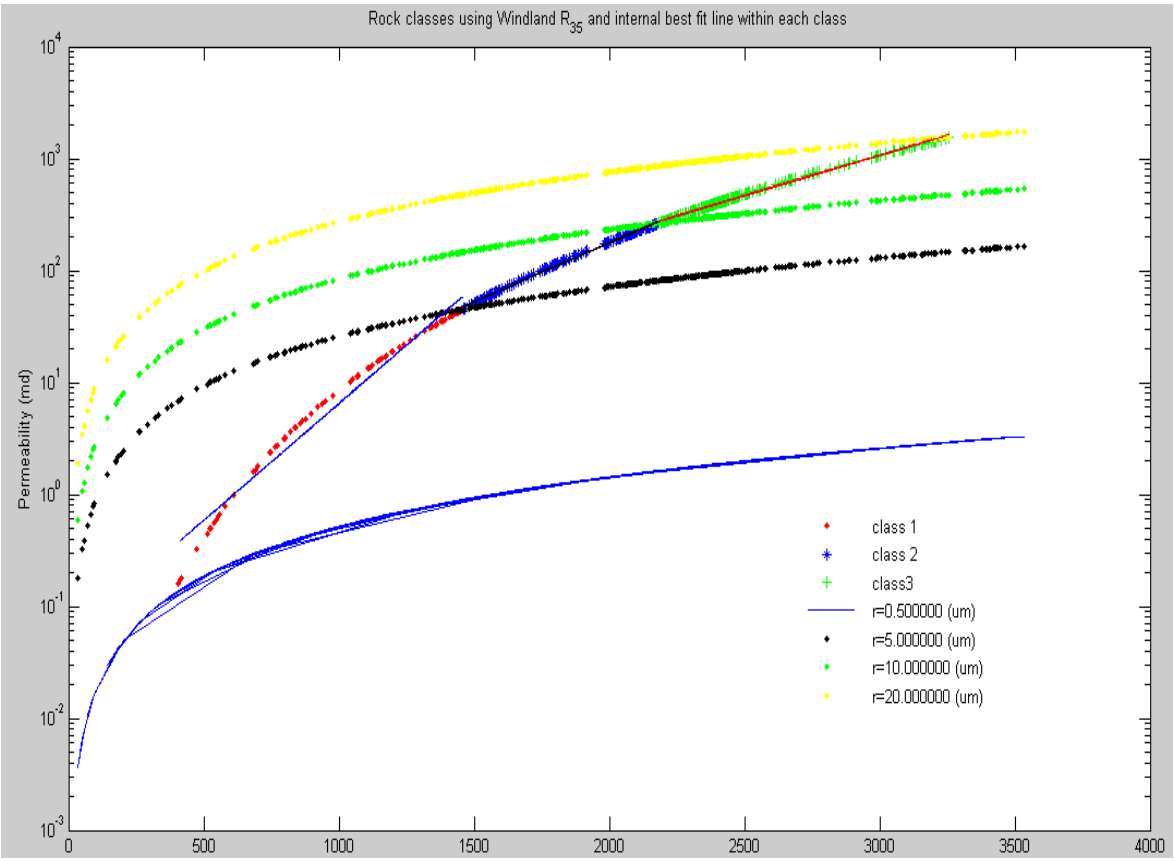

Figure 3.4: Different rock classes and the best fit between k and ϕ within each class.

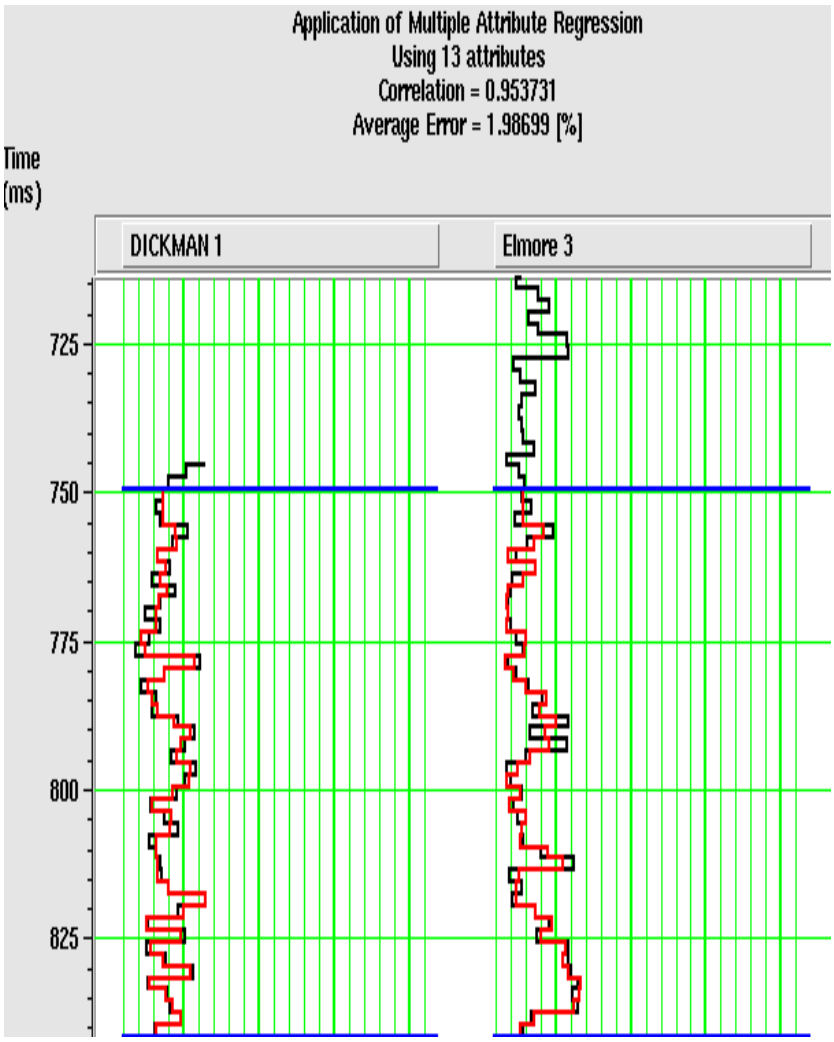

Figure 3.5: Estimated porosity (red) plotted on top of real porosity data from well logs at Dickman 1 and Elmore 3 wells showing good match with a correlation of 0.95 from a combination of 13 attributes

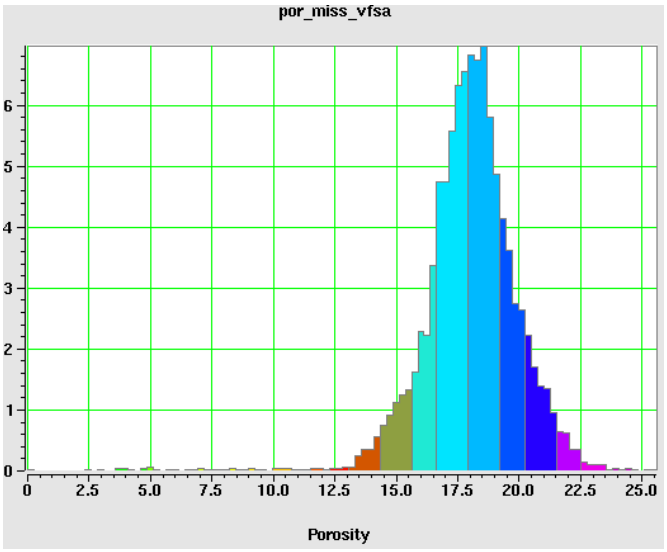

(a)

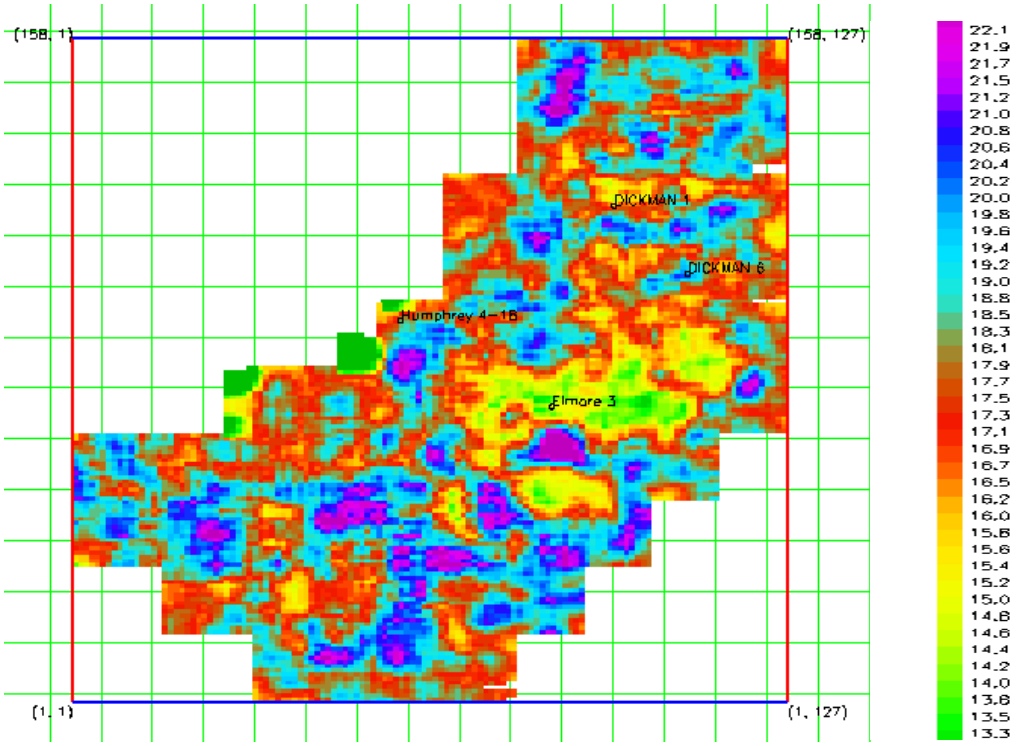

(b)

Figure 3.6: (a) Histogram of porosity values along the Miss. Carbonate shows a range between 7.5% to 25%, with an average of 18%; (b) The estimated porosity distribution along the top of the Miss. Carbonate

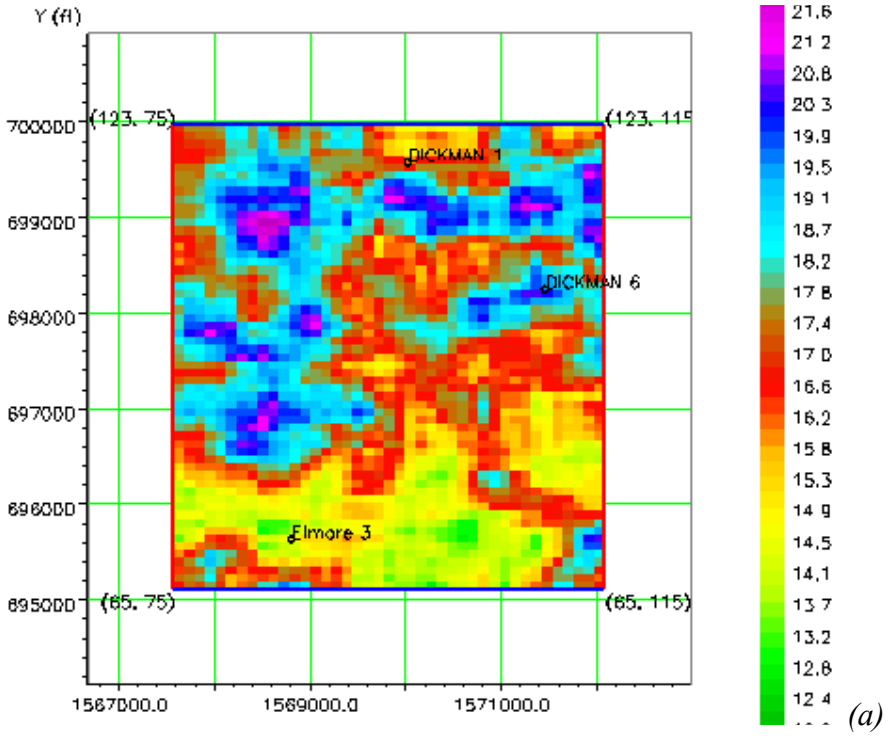

(a)

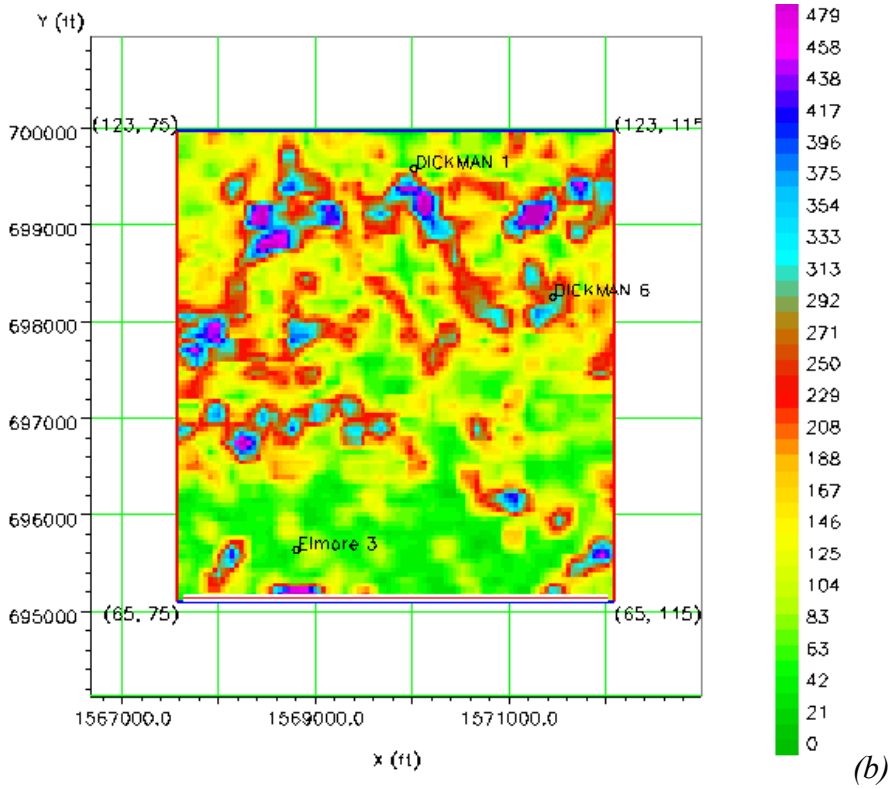

(b)

Figure 3.7: Porosity and Permeability on top of Mississippian Carbonate around the three main wells Dickman 1, Dickman 6 and Elmore 3 (a) Porosity, (b) Permeability

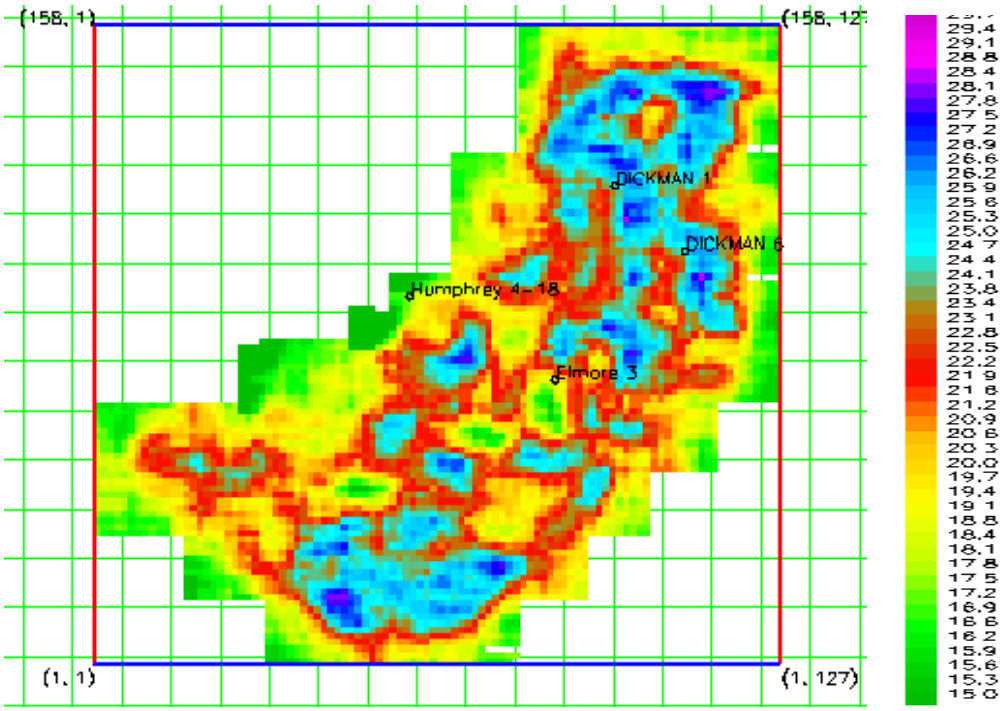

Figure 3.8: Porosity distribution on top of Gilmore formation

Chapter 4: Flow Simulation

4.1 Introduction

The purpose of performing flow simulation is to study the behavior of CO_2 as it is injected into the Carbonate Brine Reservoir, and to demonstrate how the reservoir's spatial distribution controlled by petrophysical parameters estimated from pre-stack seismic inversion effect the simulation results. Different scenarios can arise due to the chemical properties of both injecting fluid and host rock, such as solubility of injected gas (Peng and Robinson 1976), the reactions of the gas with surrounding carbonate environment (Ennis-King and Paterson, 2002; Kumar et al 2005; Obi and Blunt, 2006; Qi et al 2007), or changes in physical states of CO_2 under different temperatures and pressures.

In their study at the University of Houston, Liner et al (2009) perform flow simulation using GEM simulator from the Computer Modeling Group (CMG) to primarily predict the movements of CO_2 within the reservoir. They employ a simple injection technique where gas is injected at the bottom of an injector well. The gas is injected continuously into the formation within the first 25 years, after which the injection ceases and the migration of injected gas is simulated for another 250 years. Different trapping mechanisms are considered and included in the flow simulation. Their simulation results show that the injected gas migrates quickly vertically through the whole vertical section; with a percentage of gas concentrating near the well bore. Their conclusion is that the trapping capability is low due to the fast vertical migration of injected gas through the reservoir, and also due to a huge amount of gas that is near the well bore to follow the pipes upward.

For comparison purposes, I employ the GEM simulator from Computer Modeling Group (CMG) to perform a simulation process that accounts for all possible scenarios as mentioned above. To demonstrate how effectively the porosity and permeability estimated from previous steps can have controls in the flow simulation, I use the same injection parameters (injection rate, injection interval, chemical substances, chemical reactions…) that Liner et al (2009) used in their study. My flow simulation results will be compared directly to their work to show the quality of the reservoir models estimated from pre-stack seismic inversion and porosity estimated from multi-attribute analysis.

In this chapter, I discuss different possible trapping mechanisms that can help retain CO_2 within a reservoir, and will apply those into the flow simulation process. The fluid is injected continuously into the formation at a rate of 6.67 x 10^6 ft^3 per day (or 346 tons per day) with the maximum pressure not exceeding 5000 Pisa. The injection stops after 25 years and the flow will be simulated for 250 years. The vertical and horizontal permeability is assumed to be equal.

4.2 Method

The flow simulation process is performed on a small 3D volume surrounding three wells: Elmore 3, Dickman 1 and Dickman 6 (Figure 4.1). The first well is used as an injection well since it is located near a high porosity zone without complex geologic structures such as folds and faults. Also near the bottom of Elmore 3 well, there is a high porosity and high permeability zone favorable for injection and gas hosting (Figure 4.2).

4.2.1 Time to depth conversion

All input petro-physical parameters that affect the simulators are required to be input in field or laboratory unit expressed as a function of depth. Meanwhile, my

estimated porosity and permeability volumes are in time domain. Therefore, time to depth conversion is required before the flow simulation can run. The time to depth conversion requires a velocity model that is close to real velocity of the formations in the Dickman Field. I use a velocity volume provided with the data set, which is the migration velocity that is used for seismic imaging to remove noise and restore the seismic events to their correct location (Yilmaz et al 1987). A mathematical algorithm uses velocity values at each grid points within the velocity volume to calculate vertical depth using time value at that location. The final results are two volumes of porosity and permeability in depth domain. Figure 4.3 shows the porosity along a particular inline that passes through Elmore 3. Meanwhile, Figure 4.4 shows the permeability distribution along a vertical depth profile that cuts through the well Elmore 3.

4.2.2 Trapping Mechanisms

CO_2 injected into aquifers is trapped by four different mechanisms:

- Mineral Trapping
- Residual gas Trapping
- Solubility trapping
- Structural Trapping

The effectiveness of each mechanism is different, depending on the conditions of the reservoir and physical states of the injecting fluid. In general trapping quality improves with passage of time (Figure 4.5- ICCP 2005). Initially, the structural trapping contributes the majority of the effectiveness of the gas trapping. As time goes by, other trapping mechanisms gradually show their contributions in the overall reservoir's trapping capability.

Mineral trapping (Thibeau et al 2007) is the most permanent solution as the dissolved CO_2 in a saline aquifer decomposes into H^+ and HCO_3^-, which in turns react with containing minerals (Equation 4.1). The reaction introduces precipitation of carbonate minerals such as calcite, dolomite and siderite. However, this process is slow and minimal for the first thousand years after CO_2 injection. Possible chemical reactions are given below:

$$CO_2 + H_2O = H^+ + HCO_3^- \qquad (4.1)$$

$$CaCO_3 + H^+ = Ca^{++} + HCO_3^- \quad (4.1)$$

The residual gas trapping (Ennis-King and Paterson, 2002; Kumar et al 2005; Obi and Blunt, 2006; Qi et al 2007), is a process in which CO_2 is trapped as an immobile gas in a porous media, which is considered as safe as mineral trapping. To account for this process, I use the classical Land's residual trapping model in the CMG GEM simulator. A typical gas relative permeability curve for capturing the trapping behaviors is displayed in Figure 4.6 (Nghiem et al 2009). There are two curves in Figure 4.6: the black curve is drainage curve, while red curves are imbibition curves. Once gas saturation increases to S^*_{gi} or $S_{g,max}$ in drainage curve k^d_{rg}, the gas saturation decreases, and the gas relative permeability will follow the imbibition curves k^i_{rg}. I assume $S_{gt,max} = 0.4$ for this study (suggested by Liner 2009).

Solubility trapping is a mechanism that traps CO_2 due to its solubility in brine, especially for aqueous gas phase when it is highly soluble in brine. In general, gas solubility in aqueous phase increases with increasing pressure, but decreases with increasing temperature and salinity. With the physical condition of the host reservoir, solubility trapping is considered to be of low risk of leakage, with a small potential of

leakage due to migration of dissolved gas in water. Timothy et al (2008) reported the underground water migration speed around Dickman field to be about 40 ft. per million years, which shows that the leakage due to migration should be negligible. Therefore, it is safe to consider this trapping mechanism into simulation process. In the CMG simulator, the solubility of CO_2 into brine reservoir is calculated by solving the fugacity equation:

$$f_{CO2,aq} = f_{CO2,g},$$

Where $f_{CO2,aq}$ and $f_{CO2,g}$ are fugacity of CO_2 respectively at liquid and gas phase. The latter term is calculated using cubic equation of state and the former phase is calculated using Henry's equation:

$$f_{CO2,aq} = H_{CO2,aq}\ Y_{CO2,aq},$$

with Henry constant $H_{CO2,aq}$ and mole fraction $Y_{CO2,aq}$ of CO_2 in brine.

The last trapping mechanism is from geological structure trapping free CO_2 gas. The safety thread from this mechanism is significant as CO_2 can migrate upward to the surface through faults, fractures on cap rocks, formations or from corroded well pipes. Han et. al (2009) show that the theoretical well-pipe corrosion rates at 80F and 84 Bar are of the order of 30-60 mm/ year, which is a significant rate as the gas will likely follow the corroded pipes to reach the surface.

I include the first three trapping mechanisms discussed above into the flow simulation to study possible scenarios that can happen when CO_2 in injected into the formation. The last mechanism, due to its significant safety issue, is not incorporated in my simulation process.

4.2.3 Essential Reservoir Petrophysical Parameters

To perform flow simulation to study the behaviors of CO_2 when it is injected into a formation, I use the GEM simulator form CMG software. Input parameters are the porosity and permeability volumes calculated from previous steps. The simulator takes into account three trapping mechanisms: mineral trapping, residual trapping and solubility trapping. The injection rate was set to be 6.67 x 10^6 ft^3/day (346 ton/day) with the maximum pressure not exceeding 5000 Pisa. The injection stops after 25 years and the flow will be simulated for 275 years.

The injection field to be monitored is a small cube divided into 41 x 59 x 49 grid blocks; this includes three wells: Dickman 1, Dickman 6 and Elmore 3 (Figure 4.7). Since there is a high porosity zone near well Elmore 3, I choose this well to be the injection location. The interval inside of the well where fluid is injected into the formation is near the bottom of the well, which falls between Mississippian Carbonate and Viola (Figure 4.4). The lateral and vertical upper and lower boundaries of the cube are set to be at the same porosity and permeability values of the points nearby so that the fluid can move through, which removes the artificial seals at the boundaries.

Since this is a depleted oil field, I will assume that there are residual oil, gas, brine water and injected CO_2 to be different fluids. Figure 4.8 (a and b) shows the water and oil relative permeability curves and the gas and total liquid relative permeability curves used in the simulation. Irreducible water saturation is set to be 20%. The horizontal and vertical permeability is assumed to be the same ($k_v/k_h = 1$).

Two physical properties that control how CO_2 behaves within the reservoir are temperature and pressure. The bottom hole temperature from the well log cannot be used for formation temperature since this was measured during borehole logging; thus it is not

in equilibrium with formation temperature (Carr 2005). Instead, I use a linear function of depth to calculate the temperature at the Mississippian Carbonate (Equation 4.2a) and Deep Saline Aquifer (Equation 4.2b). Those equations (Liner 2009) are below:

$$T = 0.0131 \text{ (depth)} + 55 \text{ (Fahrenheit)} \quad (4.2a)$$

$$T = 0.0142 \text{ (depth)} + 55 \text{ (Fahrenheit)} \quad (4.2b)$$

Since the target injection zone includes both Mississippian Carbonate and Gilmore brine reservoir, I employ Equation (4.2a) to calculate temperature of the Mississippian reservoir, and Equation (4.2b) to calculate the temperature of the Gilmore reservoir. The pressure, on the other hand, follows the same equation for both Mississippian and deep saline aquifer, which is given by

$$P = 0.476 \text{ (depth) (psi/ft)}.$$

Some essential petro-physical data for Dickman field collected by Liner (2009) are:

Oil API gravity = 37 API (0.84 g/cm^3)

The reservoir temperature = 113 F

The reservoir average pressure = 2066 psia

Total Dissolved Solid Salinity = 45,000 ppm

The Aquifer water density = 1.03 g/cm^3 at reservoir condition

The reservoir water compressibility = 3 x 10^{-6} psi^{-1} at reservoir condition

4.3 Flow Simulation Results

Simulation is run for 275 years, with injection ceasing after the first 25 years. The movement of CO_2 is monitored for possible scenarios that can happen not only at the well locations but also for the entire injection field.

Well pressure recorded at Elmore 3 shows a steady increase in its value since the primary injection of the gas, and starts to decrease when injection stops (Figure 4.9). The pressure is kept under a threshold so that no artificial porosity or permeability is created, which can have significant effect on the flow simulation.

Within the first 25 years, the gas migrates upward in the vicinity near well bore. Although the well pressure does not increase after injection has stopped, CO_2 still moves within the reservoir due to pressure gradents, dispersion porosity, density contrast and overburden pressure (Figure 4.10). A large amount of gas is still concentrated around the well. Even after the injection ceases, the upward migration continue. The gas starts to migrate laterally, but a significant amount of gas is around the well.

The lateral movement of gas is displayed in Figure 4.11. The path that CO_2 follows to circulate within the reservoir is controlled strongly by porosity and permeability. Within the first 25 years, injection pressure is the primary driving factor for the fast lateral migration of injected gas. After 25 years, when injection ceases, the lateral movement is primary driven by overburden pressure, the gravity and dispersion of porosity. Within the first 100 years, the migration is fast. The gas reaches three forth of the path to Dickman 1 and Dickman 6. However, at the end of the observation period (after 275 years), the gas has not reached the two observatory wells.

4.4 Summary

My flow simulation results predict the same behaviors of the injected gas predicted from Liner et al (2009) as it is introduced into the Mississippian Carbonate formation.

The flow simulation was successfully run for 275 years. For the first 25 years, the movement of CO_2 is driven by injection pressure and the density contrast within the surrounding environment. After injection ceases, the gas movement is driven mostly by density contrast and overburden pressures. For the first one hundred years, CO_2 migrates upward due to gravity via porosity near well bore. It does penetrate throughout the whole vertical section. After this period, it starts to move laterally in all directions (Figure 4.10 and 4.11).

During the simulation process, the host rock's porosity and permeability do not change at a noticeable rate. On the other hand, the migration of CO_2 suggests a poor trapping efficiency due to small Gas Mole Fraction of this gas within the proposed target zone. Moreover, CO_2 lateral movement is much slower compared to the vertical migrations, which might be an indicator of CO_2 to penetrate through the sealing FortScott Formation. One possible explanation for the fast movement of CO_2 is the high concentration of this gas near well bore. In addition to that, CO_2 does not migrate into high porosity zone near Elmore 3 well. In addition to that, the good distribution of porosity profile along the Gilmore formation, I suggest to consider this reservoir as a new potential candidate to study its capability in doing carbon sequestration.

The consistency in simulated gas behaviors between my reservoir petrophysical models from pre-stack seismic inversion and multi-attribute analysis and that from Liner et al (2009) model from co-kriging shows the validity of the reservoir model in controlling the flow of the injected gas within the target formation.

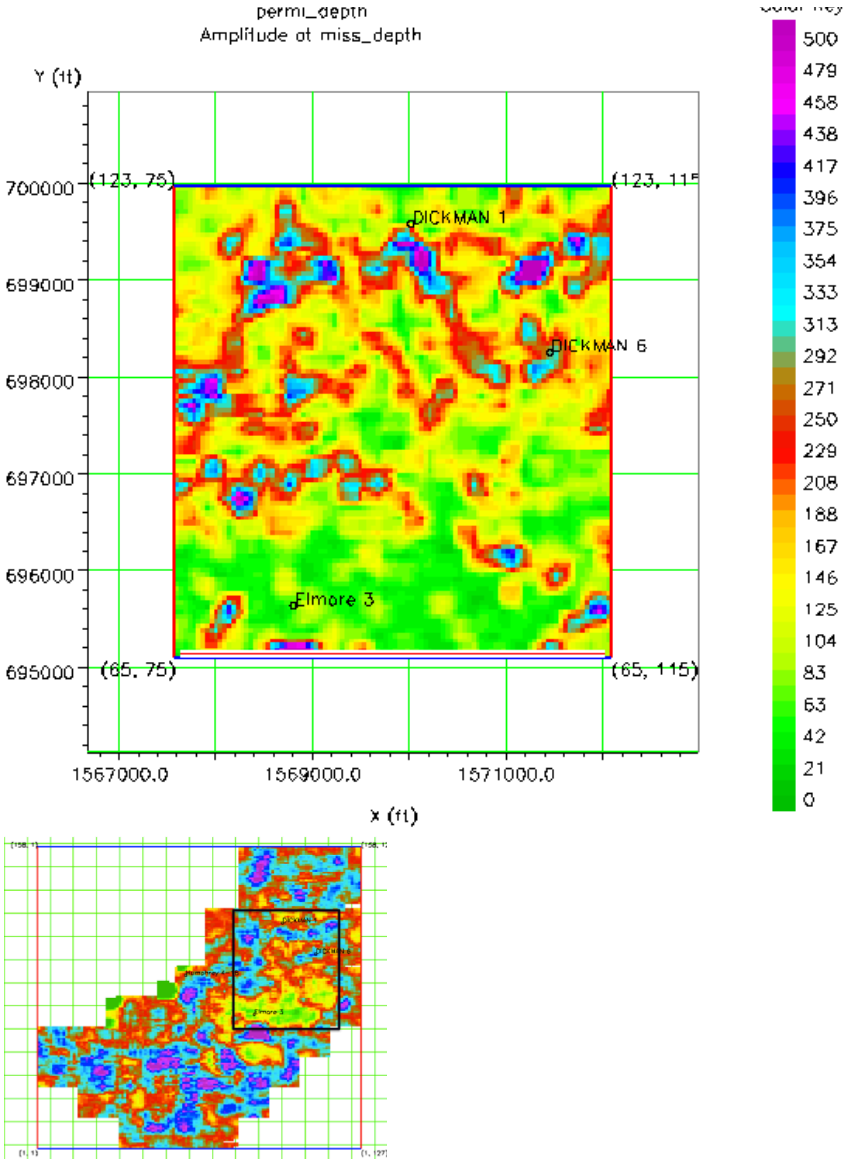

Figure 4.1: Permeability distribution of top of Mississippian carbonate throughout the small 3D cube of flow simulation (bigger picture) and its location within Dickman Field (smaller picture below)

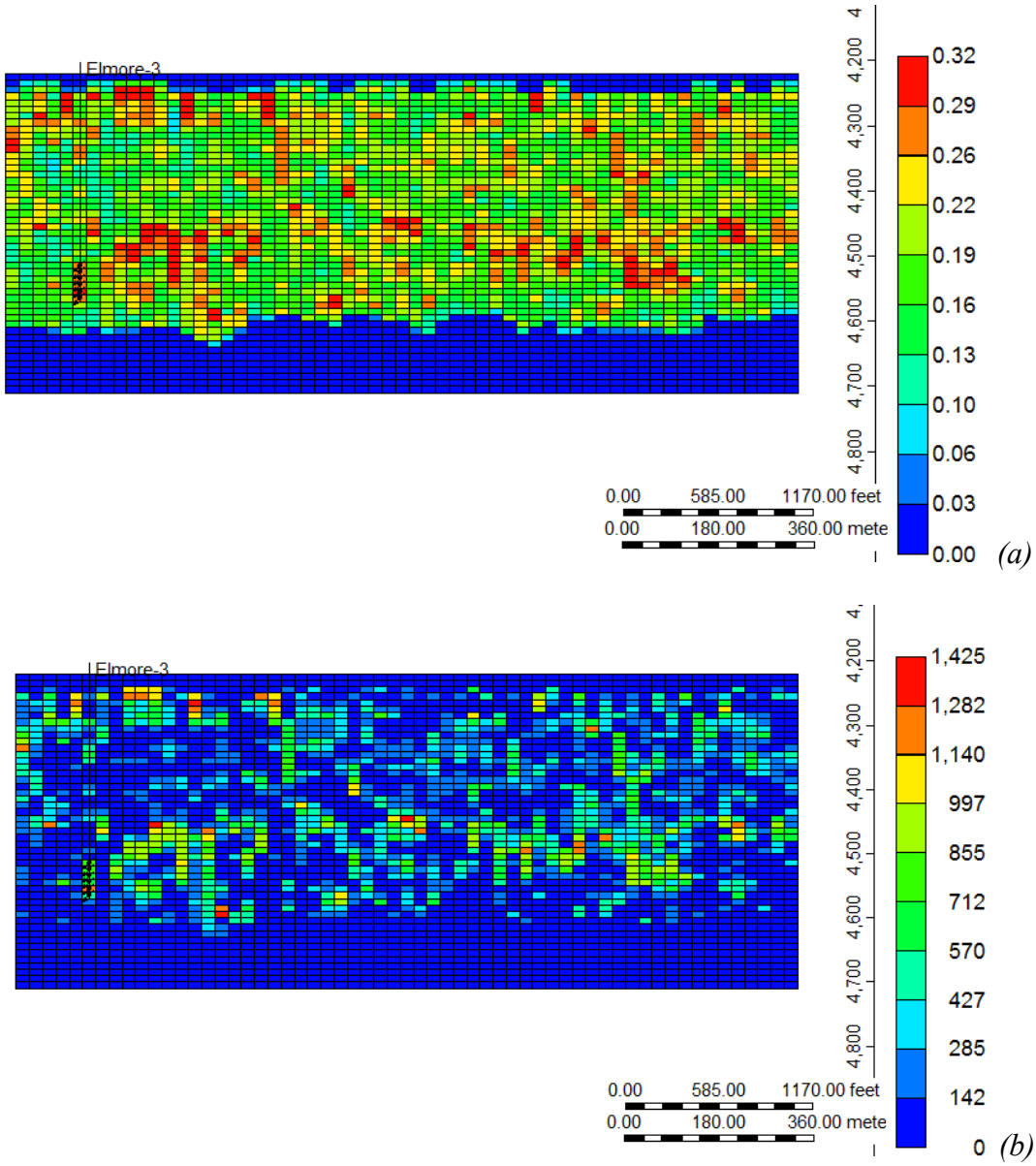

Figure 4.2: (a) Porosity distribution on an inline through Elmore 3 well. Injecting interval is chosen near the bottom of the borehole, where there is a high porosity zone; (b) Permeability distribution along the same inline showing injecting interval near a high permeability zone

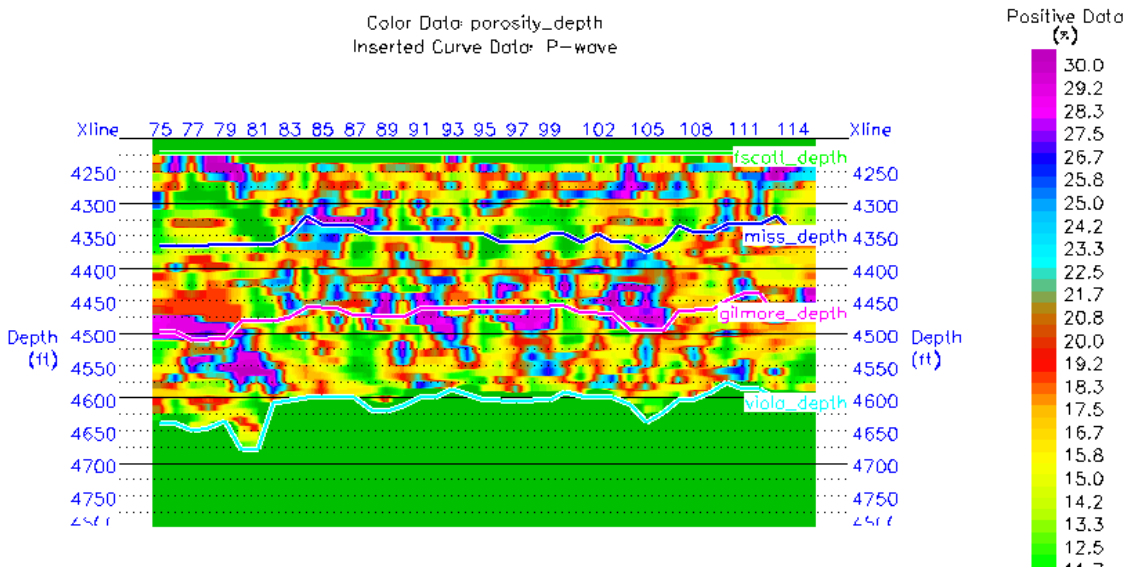

Figure 4.3: Porosity distribution along a particular inline cutting through Elmore 2 in depth domain.

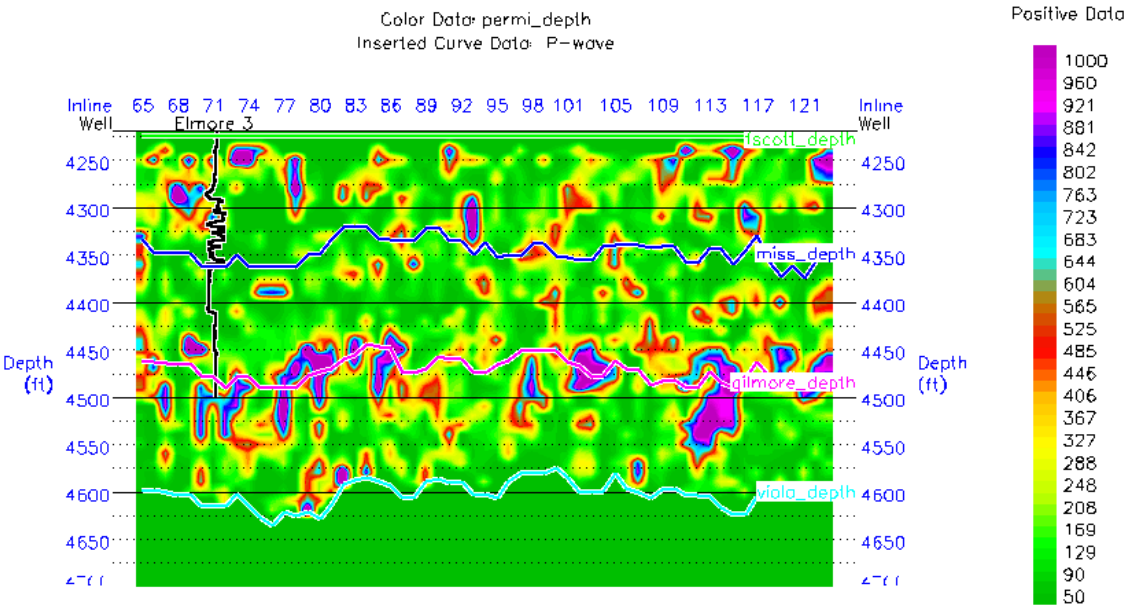

Figure 4.4: Permeability distribution along an inline cutting through Elmore 3 well in depth domain. The whole section is hung on Fortscott (in depth).

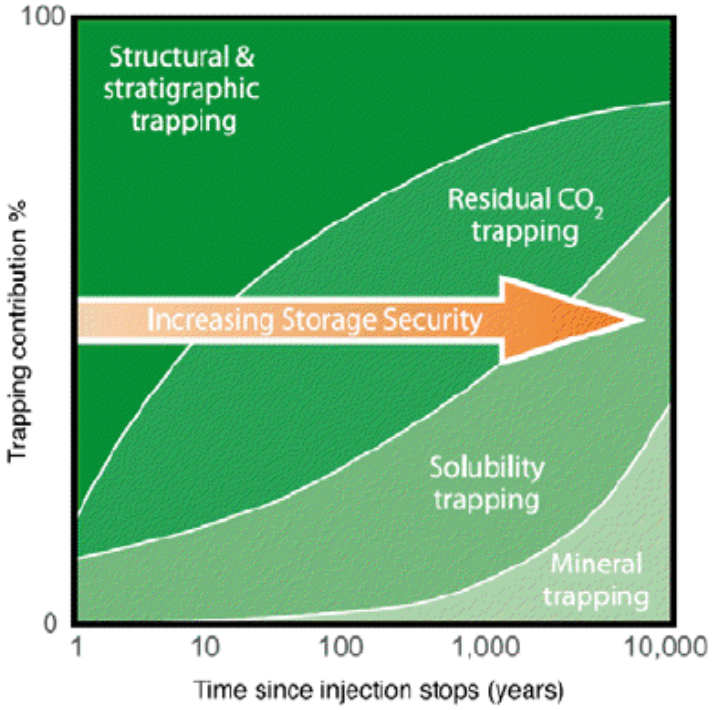

Figure 4.5: Distribution of trapping mechanism through time

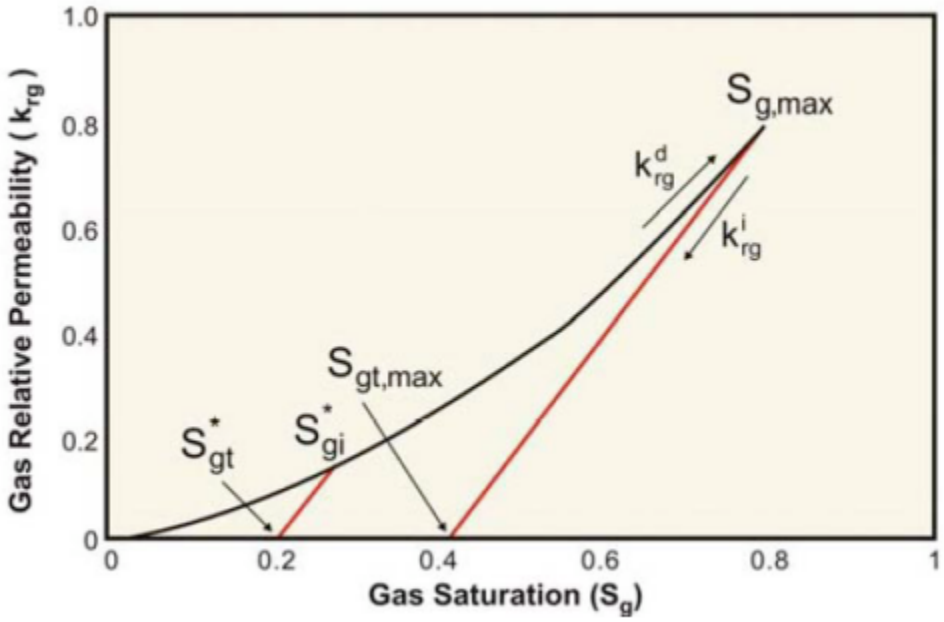

Figure 4.6: A typical Land's Residual Trapping model (Nghiem et al 2009). k^d_{rg} stands for the permeability of the gas in the drainage curve, and k^i_{rg} stands for the permeability of the gas in the imbibition curve. The saturation of the gas is represented by S_g.

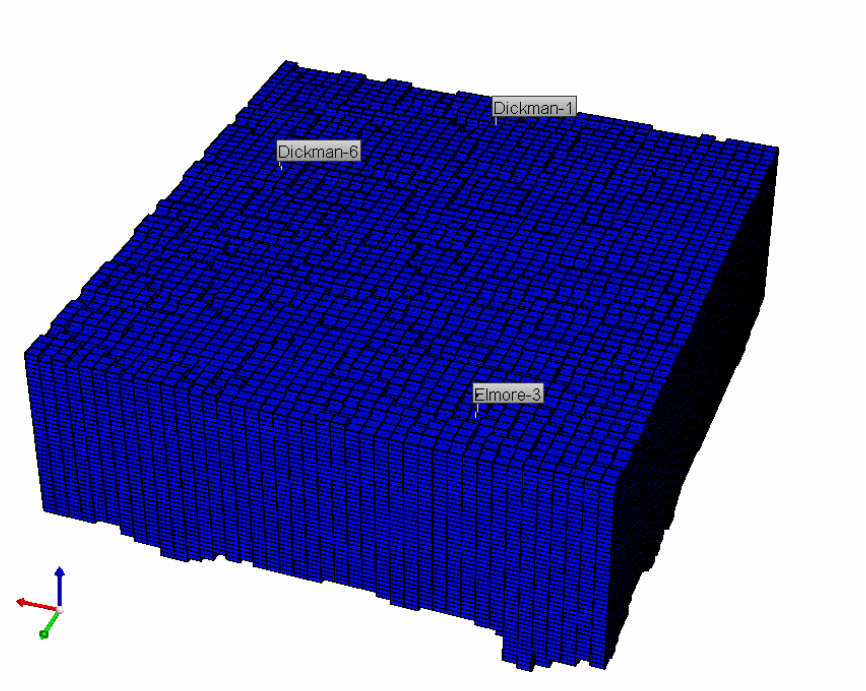

Figure 4.7: Small cube representing input volume for simulation

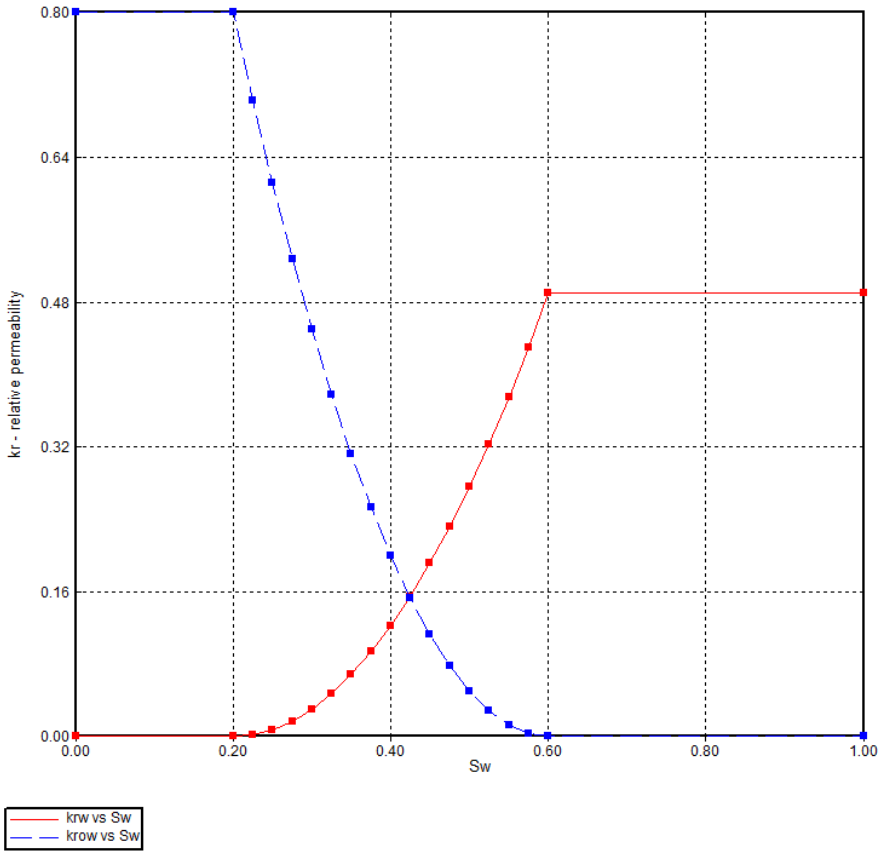

(a)

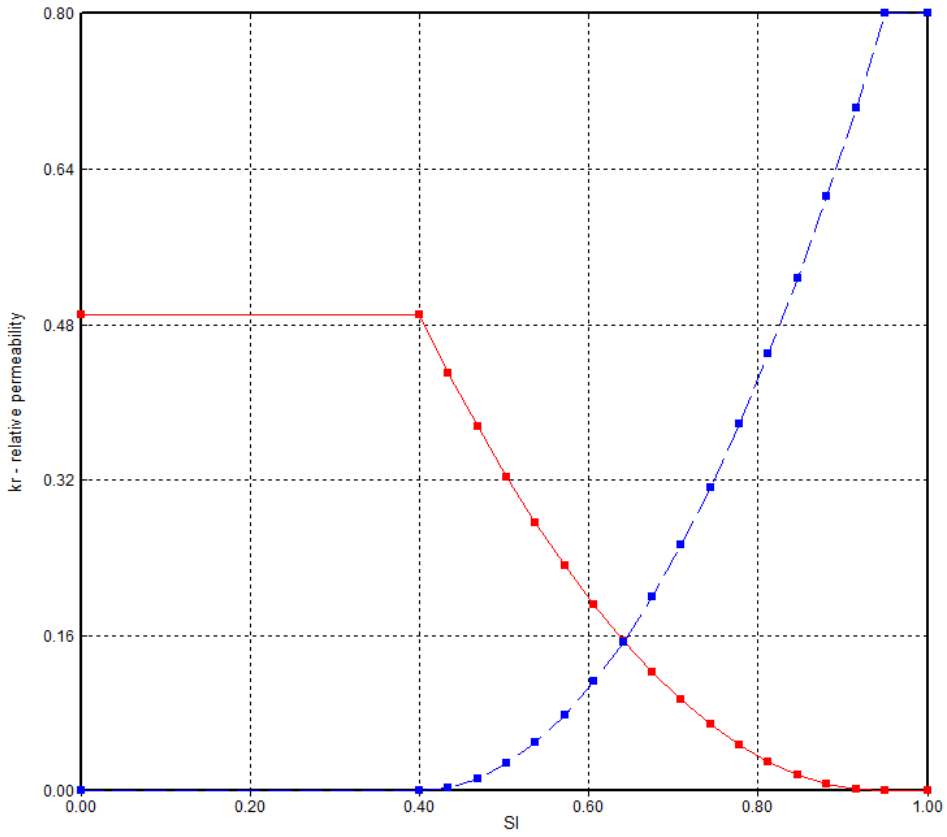

(b)

Figure 4.8: Relative permeability for different fluids (a) Oil - Water, (b) Oil - Gas

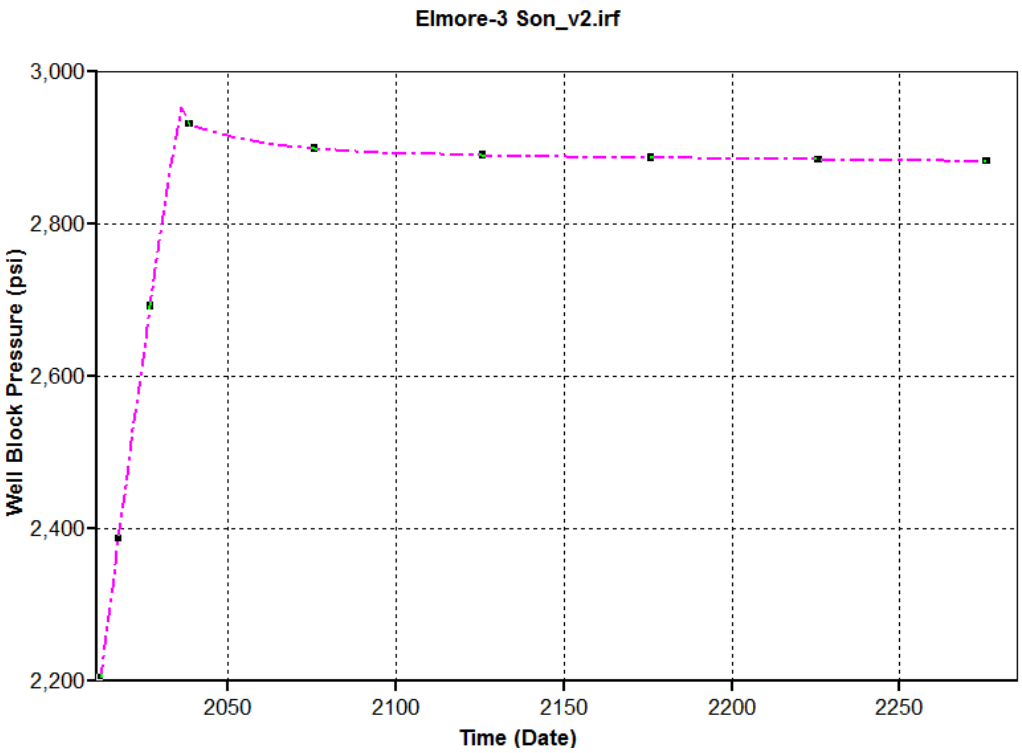

Figure 4.9: Well pressure recorded at Elmore 3 well during injection process

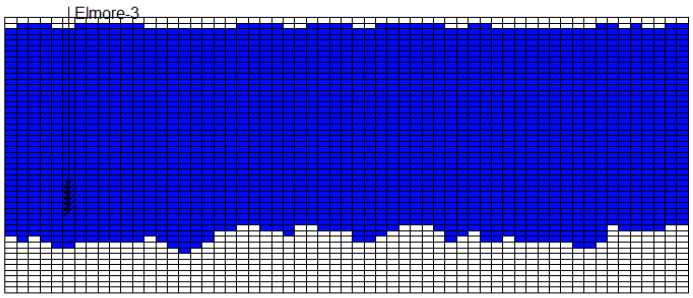

(Before Injection)

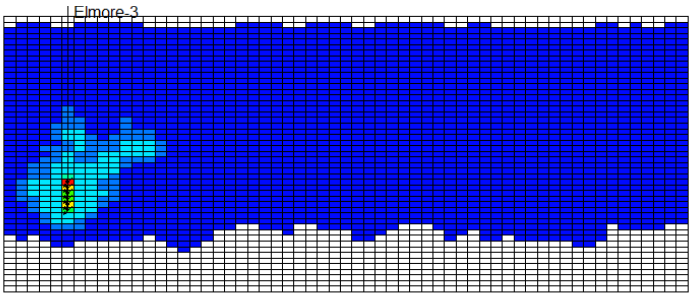

(1 year)

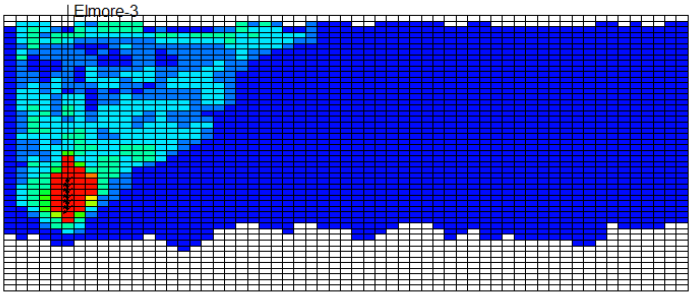

(10 years)

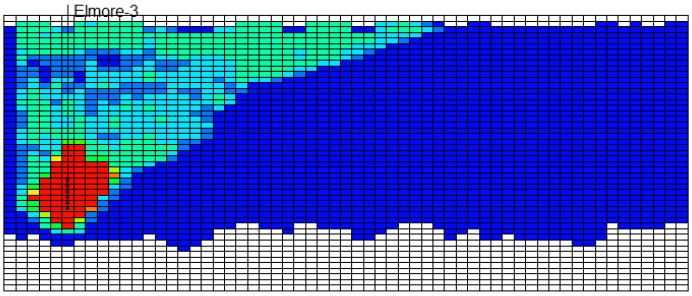

(25 years- injection ceases)

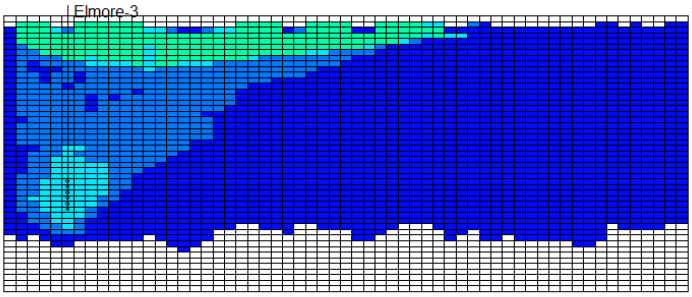

(40 years)

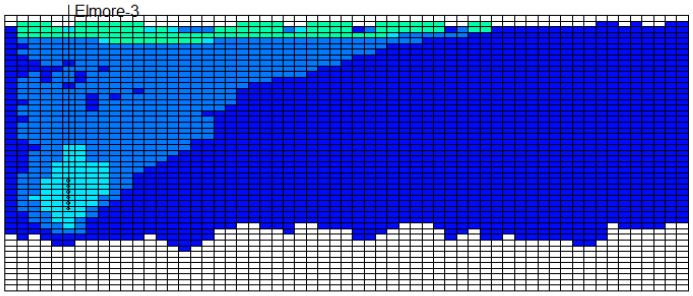

(100 years)

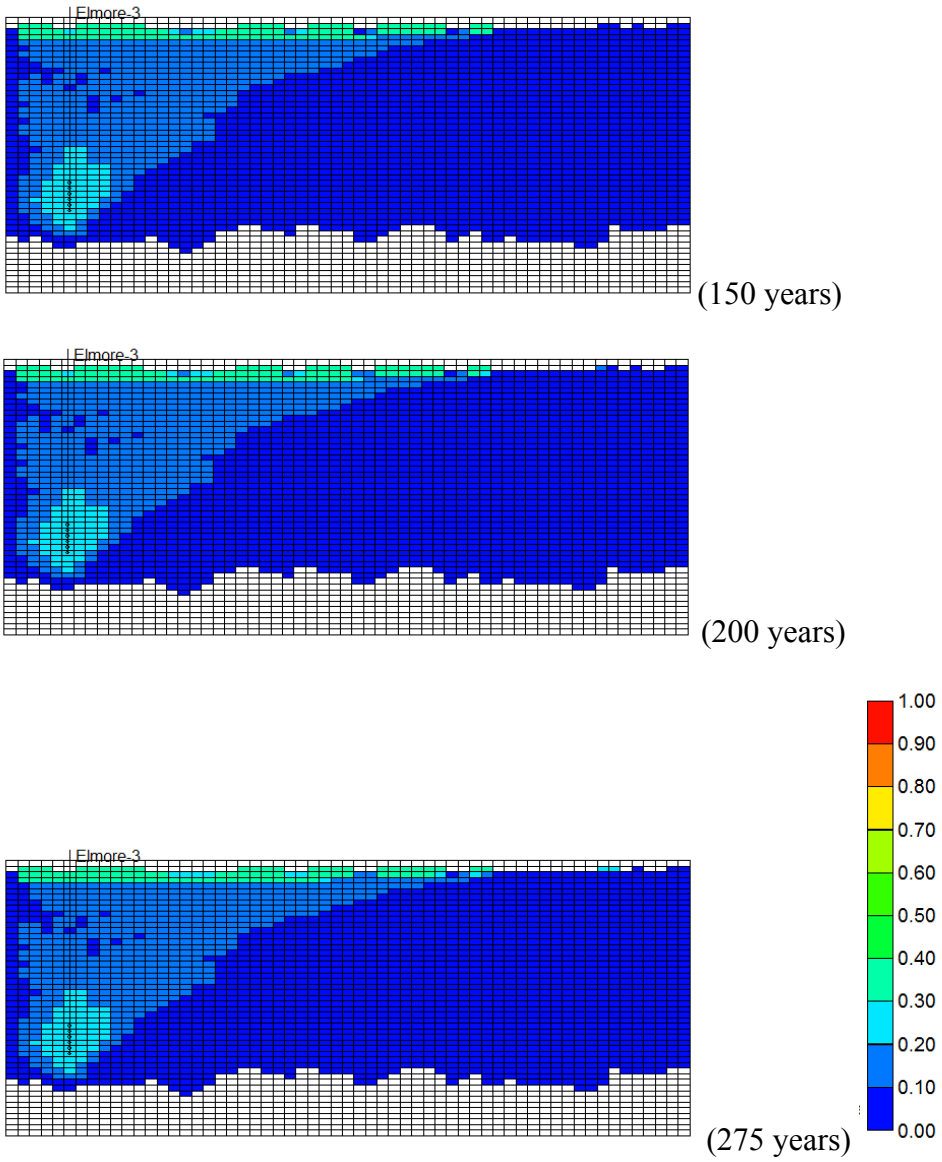

Figure 4.10: CO_2 mole fraction through time showing CO_2 movement in a vertical cross section through injecting well Elmore 3. Color bar showing the mole fraction of CO_2 during the injection time

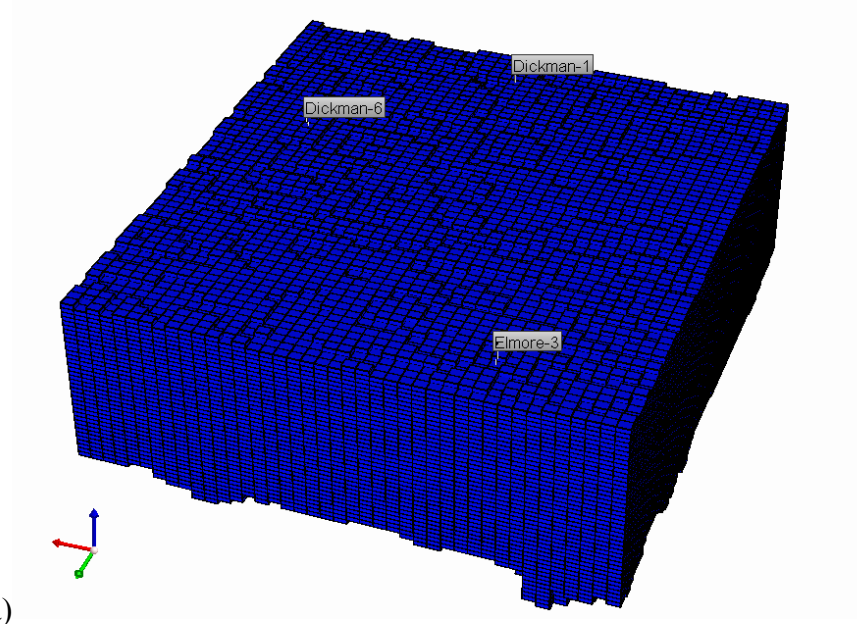

(a)

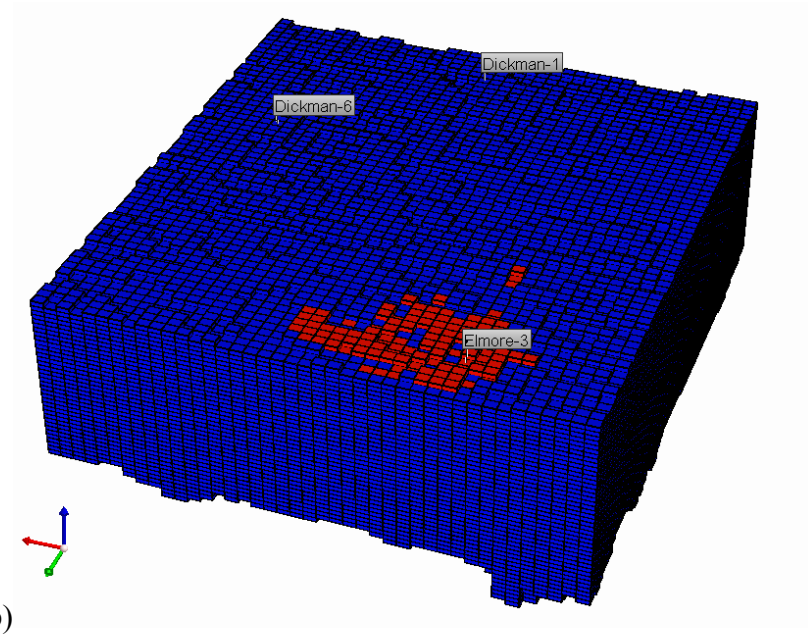

(b)

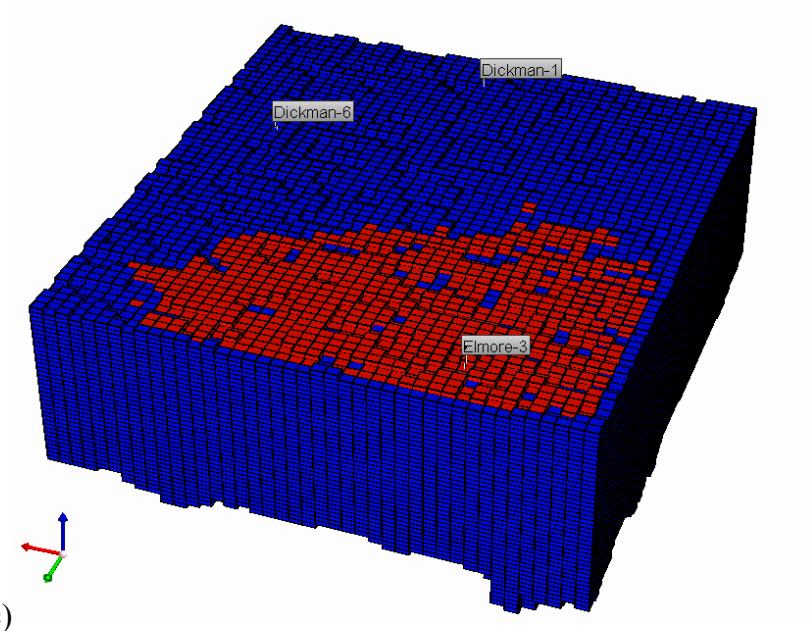

(c)

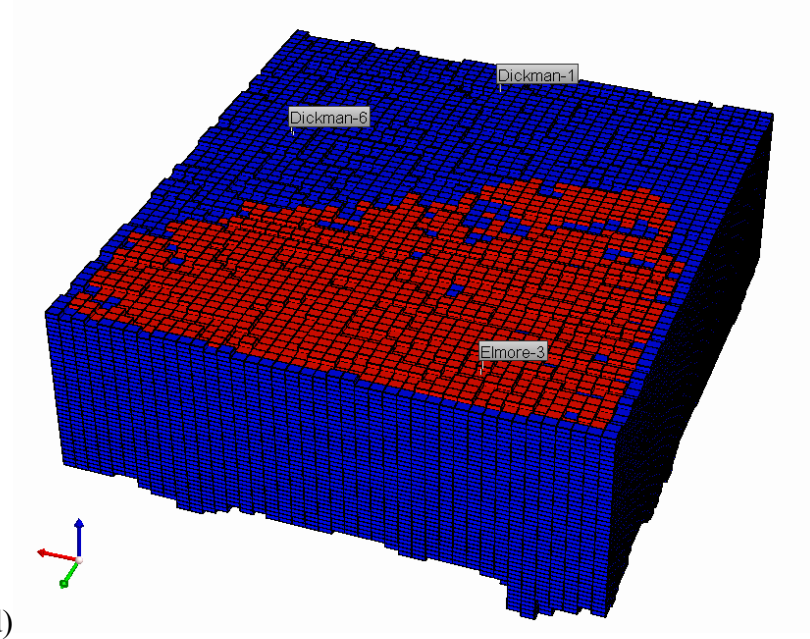

(d)

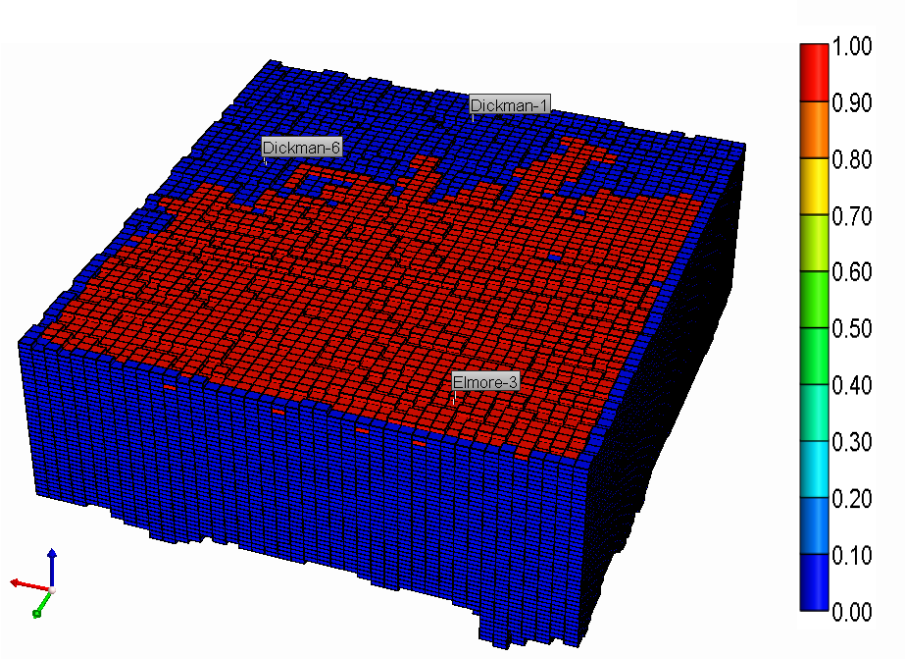

(e)

Figure 4.11: CO_2 lateral movements via Global Gas Mole Distribution of CO_2. The color scale shows the fraction of CO_2 within the formation; (a) before injection; (b) 6 years after injection; (c) after 15 years; (d) after 25 years, and injection stops; (e) after 275 years.

Chapter 5: Conclusion and Future Work

5.1 Conclusion

I was able to estimate porosity of the Mississippian Carbonate using pre-stack inversion with Very Fast Simulated Annealing (VFSA) Approach. The inversion predicted satisfactory elastic impedances (Zp and Zs), while does not predict correctly the density values (Figure 5.1). There are a few possible explanations for this. The original seismic data is only available in PP, i.e, an incoming P wave as reflected P wave. The angle range is limited to 30 degrees, which is not large enough for density contrast term in the linearized Zeoppritz equation to have any significant influence. One other possible source of uncertainty comes from the fact that I do not have available density logs from all wells used in this study. The density log at those location were estimated from sonic log using Gardner's equation; even though it fits good at well Humphrey 4-18, it may not be the correct representation of density log at the other three wells (Dickman 1, Dickman 6 and Elmore 3).

Using satisfactory inversion results, I estimate porosity using acoustic and shear impedances (Zp and Zs), density and the seismic data. The estimated porosity falls within the expected range of 7.5-25%, with an average of 18 % (Figure 5.2 and Figure 5.3). I also notice a continuously high porosity zone on top of Gilmore formation, which is a good candidate for well perforation zone (Figure 5.4).

In this study, I have successfully extracted the petro-physical properties of the Mississippian Carbonate, which is a brine reservoir, using seismic inversion and linear regression multi-attributes. The spatially distributed petro-physical parameters (porosity and permeability) estimated from seismic data to primarily evaluate the trapping are used

in a CMG flow simulation process to predict how injected CO_2 behaves within hosting formation, which helps in determining the trapping capability of that formation. Our simulation indicates a low trapping efficiency unless gas injection process (simply injecting CO_2 into the formation) is incorporate with more advanced injection techniques (water injection above gas injection zone, or horizontal well injection).

To predict the possible scenarios that can happen when CO2 is injected into the formation, I perform flow simulation. The simulation accounts for three trapping mechanisms, which are mineral trapping (the reaction between CO_2 and surrounding carbonate rocks and brine water), residual trapping for which the gas is trapped as an immobile gas, and solubility trapping when CO_2 is trapped with brine as a soluble substance. The structural trapping is not incorporated due to its high possibility of leaked gas migration to the surface. The simulation is run for 275 years, which includes continuous injection for the first 25 years, and no injection for the last 250 years. The simulation results indicate fast gas upward migration within the first 100 years, and slowly lateral migration (Figure 5.5). During the monitoring process, injected gas concentrates near well bore due to porosity there. Moreover, gas does not reach high porosity zone near perforation zone at all.

With the fast upward movements of injected gas during the first 100 years, there is high possibility of gas migration through sealing formation, or that the trapping efficiency is unsatisfactory for long-term sequestration.

In general, I observe a consistency in simulated gas behaviors between my reservoir petrophysical models from pre-stack seismic inversion and multi-attribute analysis and that from Liner et al (2009) model from co-kriging shows the validity of the

reservoir model in controlling the flow of the injected gas within the target formation. Therefore, the method employed in this study is viable and can be considered as an alternative approach to estimate and evaluate a candidate reservoir for CO_2 gas injection.

5.2 Future Work

The simulation results suggest poor trapping efficiency. Before making any further conclusion on whether the Mississippian Carbonate is not capable of trapping CO_2, it is important to test some other factors that affect the result. It is important to notice that CO_2 does not migrate into high porosity zone near the injection well, and that a large portion of this gas is still near the well bore. Therefore, a better injection technique that can separate CO_2 away from the well or to force it into the target zone is required. For the former method, one can inject brine water above the CO_2 injection zone. Water will keep CO_2 from migrating quickly upward, and also increase the solubility of this gas. As a result, less gas will concentrate near the well. On the other hand, the latter can be achieved by increasing injection pressure to force CO_2 into desired zone. However, this has to be carried out carefully in order to avoid creating artificial fractures that can trigger unpredictable migration. One other possible way is to use horizontal well toward high porosity zone before injecting CO_2.

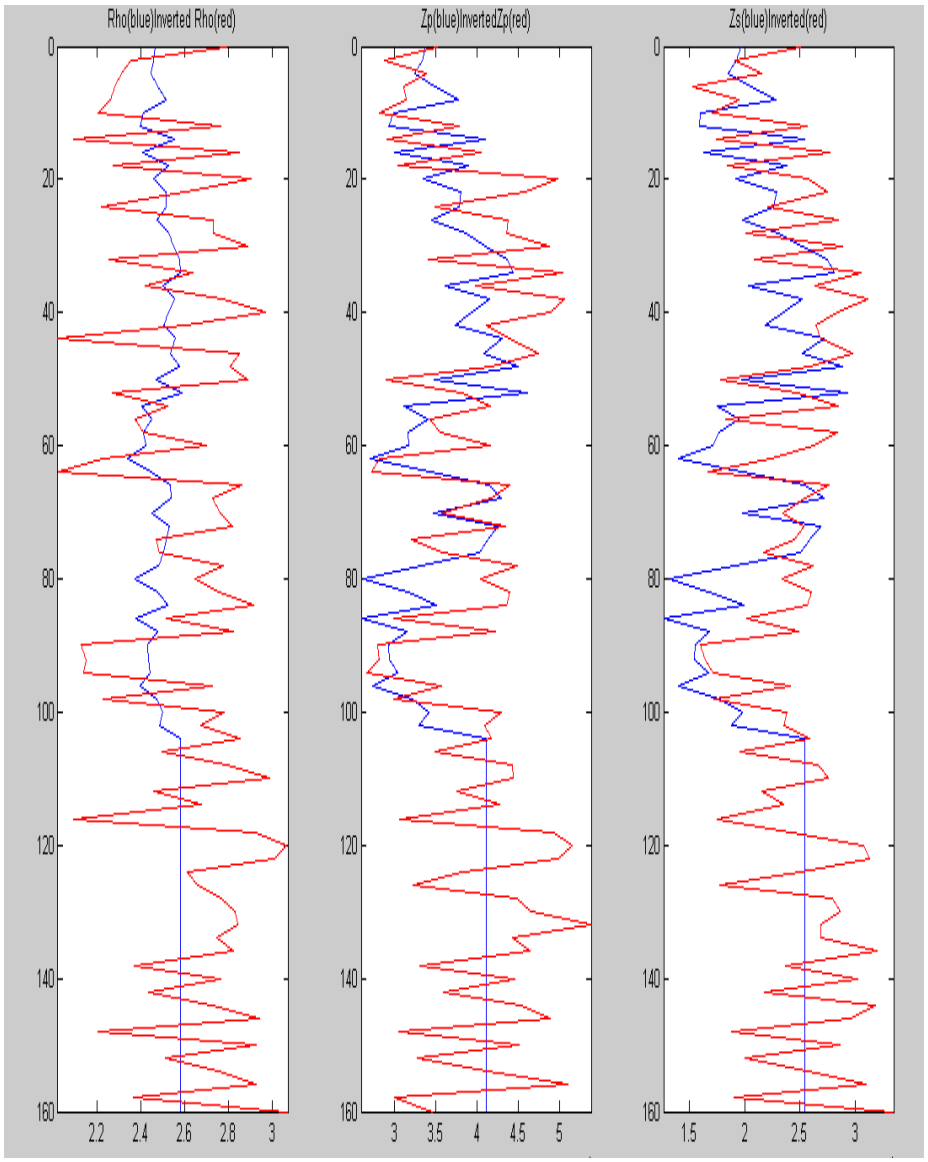

Figure 5.1: Inversion result from VFSA approach at a location. Red curves are inverted results, while blue curves are real data.

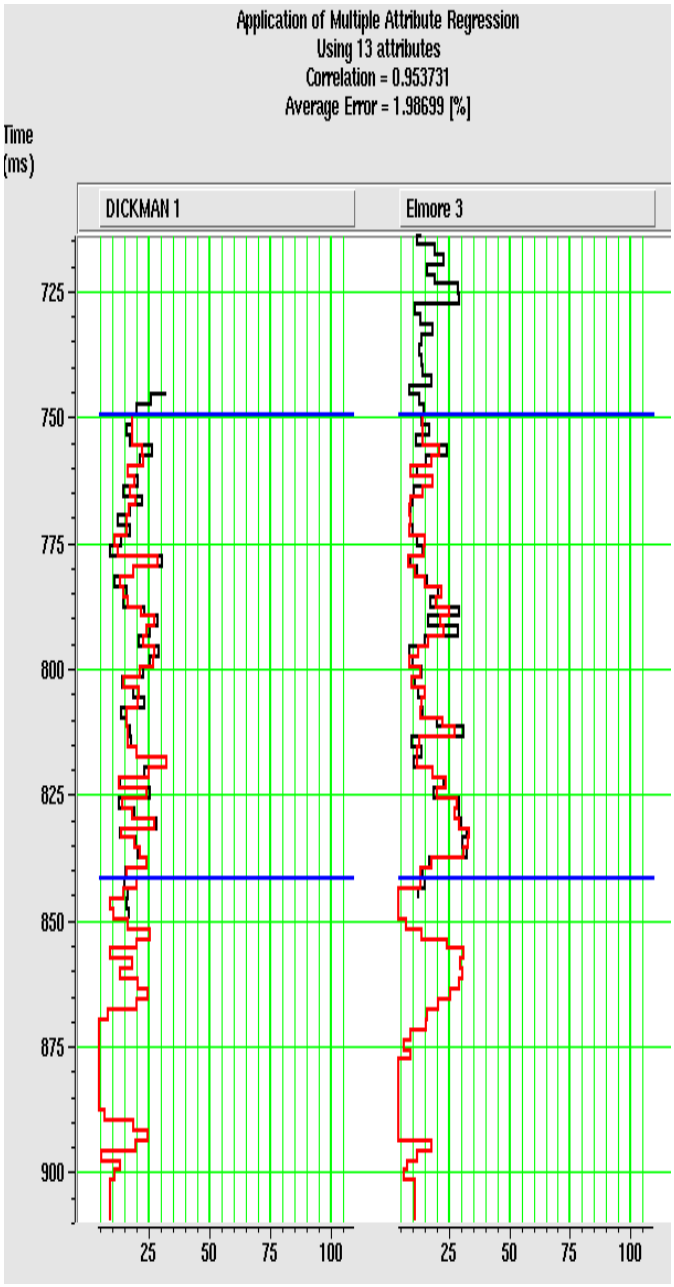

Figure 5.2: Estimated porosity (red) plotted on top of real porosity data from well logs at Dickman 1 and Elmore 3 wells showing good match with a correlation of 0.95 from a combination of 13 attributes

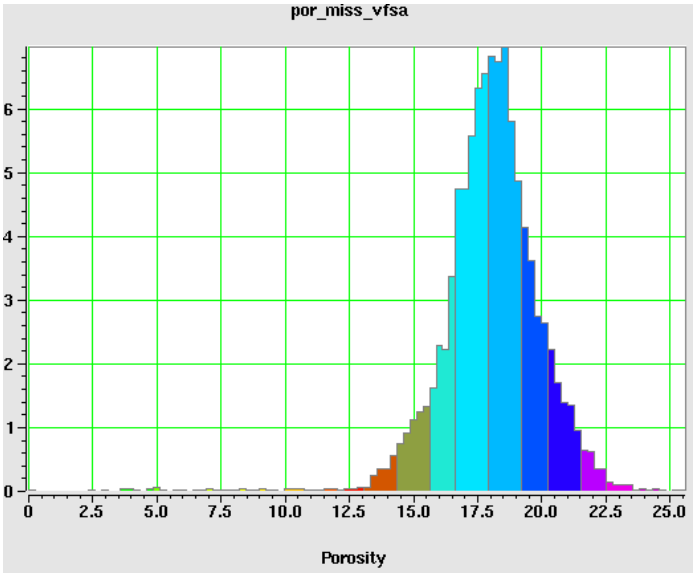

Figure 5.3: Histogram showing estimated porosity ranges from 7.5%- 25%, with an average of 18%

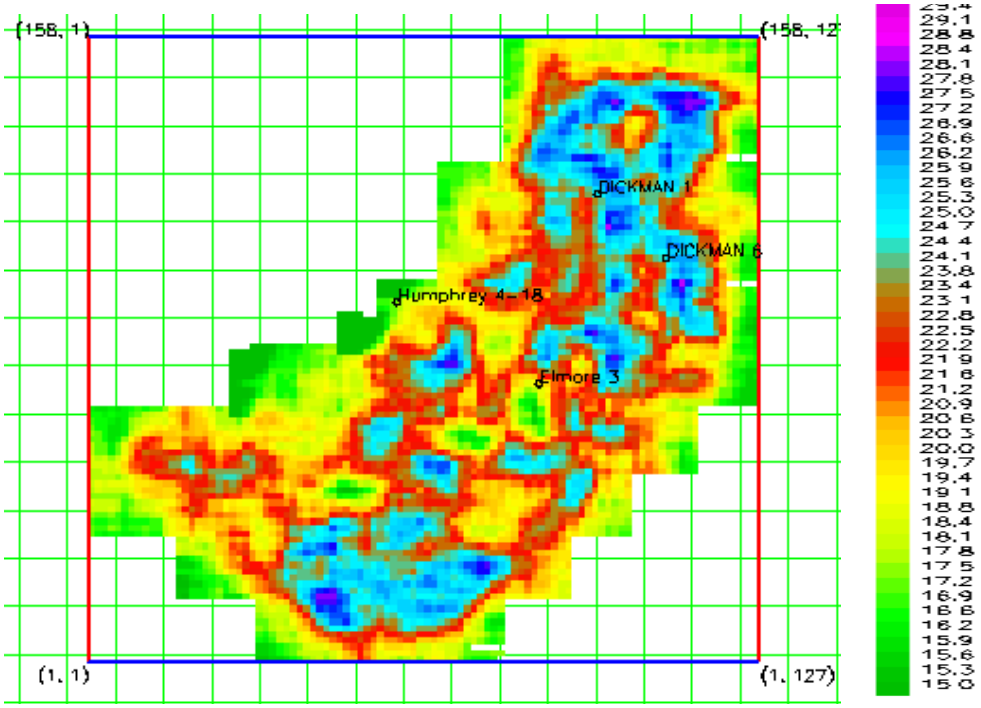

Figure 5.4: Noticeable porosity distribution along the top of Gimore Formation.

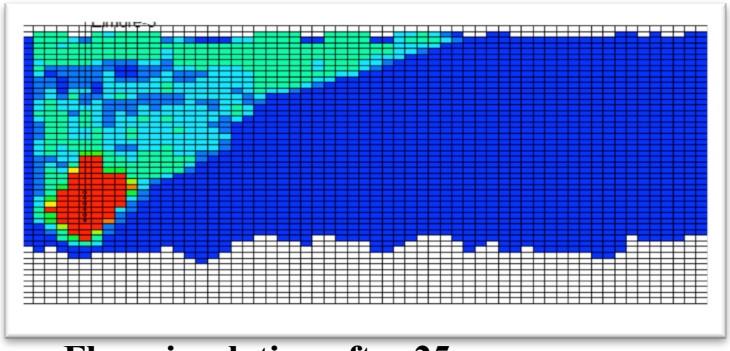

Flow simulation after 25 years

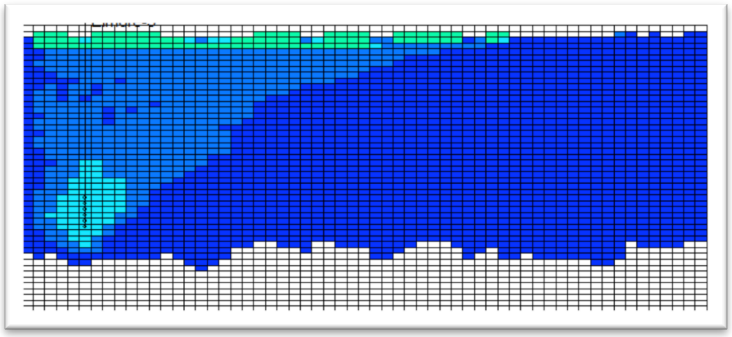

Flow simulation after 275 years

Figure 5.5: CO_2 vertical migration through time

Appendix A: VFSA Seismic Inversion Algorithm

The stochastic pre-stack inversion algorithm in this study is based on Very Fast Simulated Annealing (VFSA), which is a global optimization method that searches for a minimum of the objective function that measures data misfits and honors the statistics derived from well logs. The inversion algorithm exploits angle dependent amplitude variations to estimate Zp, Zs and density logs at each CMP locations. Here I provide an overview of the algorithm that is used to generate realistic prior using fractional Gaussian noise (Srivastava and Sen, 2010) that I implemented, and a forward modeling approach that accounts for the amplitude dependence on angle offset.

1. Fractal Based Prior Generation

The fractional Gaussian is characterized by three statistical parameters: mean, variance and Hurst coefficient, which are calculated from input data. The newly generated prior covers higher resolution estimates of the model parameters but still remain within the same frequency range of the input model.

There are many methods that can calculate the Hurst Coefficients of an input model. The method that I use for this study is called re-scaled range analysis, described best for a sufficient number of samples.

Hurst et al (1965) show a mathematical relation,

$$\frac{R}{S} = \left(\frac{N}{2}\right)^{H},$$

where R stands for the range and S stands for the standard deviation obtained from R/S analysis, N is the number of data points, and H is the Hurst Coefficients.

The R/S analysis involves creating a new series Y by adjusting an input series X with its mean value, calculating a cumulative deviate series Z of newly generated series, calculating a series of range values R of series Z and a series of standard deviation values of variable length sub-series of X. The mathematical steps of R/S analysis is summarized below:

- Calculate the mean values of input series X

  mean = $\frac{1}{N}\sum_{i=1}^{N} X_i$

- Creating new series Y

  Y(i) = X(i) – mean

- Creating cumulative deviate series Z={Z_k} for k =1,N

  $Z_k = \sum_{i=1}^{k}(Y_i - \frac{1}{k}\sum_{m=1}^{k} Y_m)$

- Calculate range series R and standard deviation series S of each sub series Z_k

  R(i) = max(Z_i) – min(Z_i)

  S(i) = std (Z_i)

The value of the Hurst Coefficient H is the slope of the best fit straight line on the plot of log(R/S) against log(N/2).

The auto-covariance of normally distributed random variables with zero mean is

$$R(\tau) = 0.5\sigma^2\left(|\tau+1|^{2H} - 2|\tau|^{2H} + |\tau-1|^{2H}\right),$$

where τ is the time step and H is Hurst Coefficient calculated above.

2. Forward Modeling

The forward modeling includes a linear approximation of the full Zeoppritz equation that Aki and Richards (1980) introduced. This computes seismic amplitude as a function of incident angle. The medium is assumed to be isotropic, homogeneous and layers with welded contact and small contrast in material properties. The re-arranged equation is first introduced by Fatti et al (1994) in terms of zero offset P-wave reflection coefficient, zero offset S-wave reflection coefficient and density contrast.

The original reflection coefficient for an incident wave is written as:

$$R_{pp}(\theta) = \left[1 + \tan^2\theta\right]R_p - \left[8\left(\frac{V_s}{V_p}\right)^2 \sin^2\theta\right]R_s - \left[\frac{1}{2}\tan^2\theta - 2\left(\frac{V_s}{V_p}\right)^2 \sin^2\theta\right]R_d, \quad \text{(A.1)}$$

$$\text{where } R_p = \frac{1}{2}\left[\frac{\Delta V_p}{V_p} + \frac{\Delta\rho}{\rho}\right], R_s = \frac{1}{2}\left[\frac{\Delta V_s}{V_s} + \frac{\Delta\rho}{\rho}\right], \text{and } R_d = \left[\frac{\Delta\rho}{\rho}\right].$$

Equation (A.1) involves Vp and Vs terms. To accommodate for impedance inversion, above equation is rewritten by following the Ma (2002) and Hampson and Russell (2005) approach:

$$L_p(i) = \frac{1}{2}\left[\ln Z_p(i+1) - \ln Z_p(i)\right], \; L_s(i) = \frac{1}{2}\left[\ln Z_s(i+1) - \ln Z_s(i)\right], \quad \text{(A.2)}$$

Replacing Rp and Rs from Equation A1 with Lp, Ls and Vp/Vs with Zp/Zs, Equation A.1 is rewritten as

$$R_{pp}(\theta) = \left[1 + \tan^2\theta\right]L_p - \left[8\left(\frac{Z_s}{Z_p}\right)^2 \sin^2\theta\right]L_s - \left[\frac{1}{2}\tan^2\theta - 2\left(\frac{Z_s}{Z_p}\right)^2 \sin^2\theta\right]R_d, \quad \text{(A.3)}$$

The convolution of reflection coefficient in Equation A.3 with angle offset dependent results in synthetic seismogram.

3. Very Fast Simulated Annealing (VFSA)

Very Fast Simulated Annealing (VFSA) is modified from simulated annealing. From physics, in a simulated annealing process, a melt cools slowly to form a crystal. The crystallization occurs at the lowest energy state, which corresponds to the global minimum of an optimization problem. Analogously, in an inverse problem, the melt corresponds to a set of model parameters; the annealing temperature is analogous to the controlling parameters that determine the acceptance or rejection of the model parameters; while the crystallization energy state of the material refers to the global minimum error.

Traditionally, the sampling algorithm is based on the direct Monte Carlo search of the model parameters within a preset upper and lower bounds (Metropolis et al 1953, Kirkpatrick et al 1983). The modified algorithm called very fast Simulated Annealing (VFSA) was first proposed by Ingler (1989) and implemented by Sen and Stoffa (1995). The algorithm converges faster than the previous variants of Simulated Annealing algorithms of Geman and Geman (1984) or Szu (1987). The VFSA uses a Cauchy like distribution to span the model space, and follow a cooling scheme (Equation A.4) where T_i is the temperature of the i^{th} parameter in k^{th} iteration and T_o is the starting global temperature, c is a decay parameter.

$$m_i^{k+1} = k_i^{k} + y_i\,(m_i^{\max} - m_i^{\min}), \qquad \text{(A.4)}$$

where,

$$y_i = \operatorname{sgn}(u_i - 0.5)\, T_i \left[\left(1 + \frac{1}{T_i} \right)^{|2u_i - 1|} - 1 \right],$$

$$T_i(k) = T_0 \exp(-c_i k^{d_i}),$$

ui is a random parameter between [0, 1] generated for each i^{th} parameter, c_i and d_i are two decaying parameters that control the temperature decay pattern.

The forward modeling (Appendix A, part 2) follows using an updated model, and the error is calculated for the new model. The decision on accepting/ rejecting new model update is dependent on a probability function given by:

$$P = \exp\left(-\frac{\Delta E_i}{T_i}\right), \qquad \text{(A.5)}$$

where ΔE is the difference in error between two consecutive iterations. Commonly, a new model is accepted when error of the new model is lower than error of the previous model. However, in VFSA, a new model is sometimes accepted even if the error is greater than that of previous model. This acceptance scheme makes the algorithm robust and avoids it to be trapped at local minimum.

4. The Objective Function

The objective function compares the synthetic data with real data that constrain the inversion algorithm. I employ a normalized objective function that accounts for the effects of different parameters (seismic data, mean μ and standard deviation σ of input data, and the Hurst coefficient of new models

$$E = 2\frac{\sum|obs-cal|}{\sum|obs+cal|+\sum|obs-cal|} + \alpha\frac{|\mu-\mu_{new}|}{|\mu+\mu_{new}|^2} + \beta\frac{|\sigma-\sigma_{new}|}{|\sigma+\sigma_{new}|^2} + \gamma\frac{|H-H_{new}|}{|H+H_{new}|^2},$$

where α = 0.001, β = 0.0025, γ = 0.0025.

Bibliography

Angeleri, G, Carpi, R, 1982, *Porosity prediction from seismic data*, Geophys. Prosp., 30, 580- 607

Arts, R, Eiken, O, Chadwich, A, Zweigel, P, Van Der Meer, L, Zinszner, B, *Monitoring of CO_2 injected at Sleiper using time- lapse seismic data*, Energy, Vol. 29 2004

Castagna, J.P., Batzle, M.L., and Eastwood, R.L., 1985, *Relationships between compressional-wave and shear-wave velocities in clastic silicate rocks*: Geophysics, 50, 571-581

Carr, T. R., D. F. Merriam, and J. D. Bartley, 2005, *Use of relational databases to evaluate regional petroleum accumulation, groundwater flow, and CO_2 sequestration in Kansas*, AAPG Bulletin, 89, 12, 1607–1627

Castagna, J, Batzle, M, Eastwood, R, 1985, *Relationship between compressional-wave and shear-wave velocities in clastic silicicates*, Geophysics, 50 (4), P. 571-581

Delepine, N, Clochard, V, Labat, K, Ricarte, P, and Le Bras, C, 2009, *Stratigraphic inversion for CO2 monitoring pruposes- A case study for the saline aquifer of Sleiper Field*, EAGE Extended Abstracts

Doyen, P, 1988, *Porosity from Seismic data: A Geostatistical Approach*, Geophysics, Vol. 53, N0. 10, October, 1263-1275

Gardner, G, Gardner, L, Gregory, A, 1974, *Formation velocity and density – the diagnostic basics for stratigraphic trap*s: Geophysics, 39, 770- 780

Geman, S., and Geman,D., 1984, *Stochastic relaxation, Gibbs distributions, and the Bayesian restoration of images*: IEEE Transactions in Pattern Analysis and Machine Intelligence, **6**, 721-741.

Ghosh, R, Sen, M, 2011, *Predicting subsurface Co2 movement: from laboratory to field scale*, Geophysics, submitted

Hampson D.P., J. S. Schuelke, and J. A. Quirein, 2001, *Use of multi-attribute transforms to predict log properties from seismic data*, Geophysics, 66, 220–236

Ingber, L., 1989, *Very fast simulated re-annealing*: Mathematical Computational Modeling, 12, 967-973.

Han, J; Carey, J and Zhang, J, 2009, *A coupled water chemistry and corrosion model for high salinity-high CO2 environments with application to wellbore integrity in CO2 sequestration*, Eos Trans. AGU, 90(52), Fall Meet. Suppl., Abstract H11J-04

Kolodziek S; 1980; *Analysis of pore throat size and use of the Waxman-Smits equation to determine OOIP in Spindle Field*, Colorado: SPE 9382

Kumar, A, Ozah, R, Noh, M, Pope, G, Bryant, S, Sepehrnoori, K and Lake, L, *Reservoir Simulation of CO2 Storage in Deep Saline Aquifers*, SPEJ, Vol 10 (Sep 2005), 336-348

Lindseth, R; 1979; *Synthetic Sonic Logs – a process for stratigraphic interpretation; Geophysics*, 44, P. 3- 26

Land, C, 1968, *Calculation of Imbibition Relative Permeability for Two- and Three-Phase Flow from Rock Properties*, SPEJ, Vol. 8, No. 2, 149-156

Liner, C, Geng, P, Zeng, J, King. H, Li, J, Flinn, B, LeBlanc, S; *Application of Cutting-Edge 3D Seismic Attribute Technology to the Assessment of Geological Reservoirs for CO2 sequestration; Quarterly Report (October 2009- December 2009),* DOE DE- FG26-06NT42734

Liner, C. L., P. Geng, J. Zeng, and H. King, 2009, *Toward flow simulation for CO_2 sequestration at the Dickman Oilfield*, Ness Co.,Kansas, SEG Expanded Abstracts 28, 3559, DOI:10.1190/1.3255604.

Lumley, D, *4D seismic monitoring of CO2 sequestration*, The Leading Edge, Vol. 29, No. 02, 2010

Ma, J, Morozov, I, *AVO modeling of pressure- saturation effects in Weyburn CO_2 sequestration*, The Leading Edge, Vol. 29, No. 02, 2010

Metropolis, N., Rosenbluth, A.W., Rosenbluth,M.N., Teller, A.H., and Teller, E., 1953, *Equation of state calculations by fast computing machines*: Journal of Chemical Physics, 21, 1087-1092.

Miller, S and Stewart, R, 1991, The relationship between elastic-wave velocities and densities in sedimentary rocks: A proposal, CREWES 1991 Research Report, pg 260-273

Nghiem, L; Yang, C; Shrivatava, V; Kohse, B; Hassam, M; Chen, D and Card, C, 2009, *Optimization of Residual Gas and Solubility Trapping for CO_2 Storage in Saline Aquifer*, SPE 119080

Pedersen, K; Fredenslund, A and Thomassen, 1989, *Properties of Oils and Natural Gas*, Gulf Publishing Company, Pg. 99- 112

Resnick, J, 1993, *Seismic data processing for AVO and AVA analysis*, in J.P. Castagna and M. M. Backus, ed., Offset-dependent reflectivity: Theory and practice of AVO analysis: SEG Investigation in Geophysics, NO. 8, 175-189

Sayers, C, Wilson,T, 2010, *An introduction to this special section: CO_2 sequestration*, The Leading Edge, Feb, PG 149-149

Schultz, P, Ronen, S, Hattori, M, Corbett, C, 1994, *Seismic guided estimation of log properties*, parts 1, 2, and 3, The Leading Edge, VOl 13, 305-310, 674-678, 770-776

Sen, M. K., and Stoffa, P.L., 1996, *Bayesian inference, Gibbs' sampler and uncertainty estimation in geophysical inversion*: Geophysical Prospecting, 44, 313-350.

Srivastava, R; Sen, M; 2010; *Stochastic Inversion of prestacked seismic data using fractal-based initial models*; Geophysics, 75, R47-R59

Szu, H., and Harley, R., 1987*, Fast simulated annealing*: Physics Letters A, 122, 157-162.

Timur, A; 1968; *An investigation of permeability, porosity and residual saturation relationship*, Trans SPWLA 9th Annual Logging Symposium Paper K, P. 15

Todd, C and Backus, M, 1985, *Offset-dependent reflectivity in a structural context*, SEG 55th Annual International Meeting, SEG Expanded Abstracts, 586- 588

Urosevic, M, Pevzer, R, Kepic, A, Wisman, P, *Time- lapse seismic monitoring of CO_2 injection into a depleted gas reservoir- Naylor Field, Australia*, The Leading Edge, 2010, Vol. 20, No. 02

Vanorio,T, Mavko, G, Vialle, S, Spratt, K, *The rock physics basis for 4D seismic monitoring of CO_2 fate: Are we there yet?*, The leading Edge, 2010, Vol. 29, No. 02

Yilmaz, O, Doherty, S, 1987, *Seismic Data Processing*, SEG, Vol 2

Zarantonello, S, Bevc, D, Harris, J, 2010, *Integrated reservoir, petrophysical, and seismic simulation of CO_2 storage in coal beds*, The Leading Edge, Feb, Pg 184-190

Vita

Son Phan was born in Vietnam in December 08, 1986. Son graduated from Le Quy Don High School for the gifted with a bronze medal in Physics in the Olympic Competition for gifted students in the Southern part of Vietnam. Son came to the University of Tulsa in Tulsa, Oklahoma to study geophysics and applied mathematics with a full scholarship for best high school students from PetroVietnam. In 2009, Son graduated with a Bachelor of Sciences in Geological Sciences with the A.N. Murray Award for Outstanding achievement in Geosciences, and a Bachelor of Sciences in Mathematics with the Ralph W. Veatch Award Certificate for outstanding academic achievement in Mathematics. Son joined Continental Resources Inc. in Summer 2008 to work as an intern geophysicist in Enid, Oklahoma. In the Spring Semester of 2009, Son worked at the Society of Exploration Geophysicist Headquarter in Tulsa, Oklahoma as an academic training student. In June of 2009, Son joined the Institute for Geophysics to work as a research assistant under the supervision of Professor Mrinal K. Sen. In August of 2009, Son entered the graduate program at Jackson School of Geosciences, The University of Texas at Austin. Son was primarily supported by a research grant from the U.S Department of Energy. In academic year of Fall 2010- Spring 2011, Son received the Chevron Texaco fellowship. Son will be working with PetroVietnam in Vietnam after graduation.

For contact information, Son can be reach at sonphanut@gmail.com

This thesis was typed by the author.